Chinese Chemical Letters 31 (2020) 2525–2538

Contents lists available at ScienceDirect

Chinese Chemical Letters

journal homepage: www.elsevier.com/locate/cclet

Review

Recent advancements in graphene adsorbents for wastewater treatment: Current status and challenges

MD Faysal Hossain[a], Nasrin Akther[a], Yanbo Zhou[a,b,*]

[a] State Environmental Protection Key Laboratory of Environmental Risk Assessment and Control on Chemical Process, East China University of Science and Technology, Shanghai 200237, China
[b] National Engineering Laboratory for Industrial Wastewater Treatment, East China University of Science and Technology, Shanghai 200237, China

ARTICLE INFO

Article history:
Received 11 March 2020
Received in revised form 9 April 2020
Accepted 10 May 2020
Available online 15 May 2020

Keywords:
Wastewater
Adsorption
Graphene composites
Interaction mechanism
Regeneration

ABSTRACT

From emerging pollutants to emerged threat, researchers are continuously looking for promising technologies for wastewater treatment. Adsorption has been identified as the most convenient approach for treating wastewater at low-cost and with high-efficiency. Recently, graphene and its derivatives have gained heightened attention as novel adsorbents because of their unique molecular structure and outstanding physicochemical properties. Heavy metals, dyes, polycyclic aromatic hydrocarbons (PAHs) and other pollutants, which are widely concerned recently, all show different adsorption behaviors. Numerous functional groups, resonating and delocalized π-electron system of graphene derivatives lead to the formation of various adsorptive interactions *i.e.*, π-π interactions, electrostatic interactions, H-bonding, *etc.* with these venomous pollutants, and quarantine them in solution. The pristine form of graphene subsidiaries tends to exhibit low sorption efficiency due to high propensity of agglomeration, lack of selectivity, hydrophobicity and difficulty in phase separation after treatment. Therefore, designing of efficient graphene composites through the surface modification with numerous functional groups, polymers or nanoparticles is an ongoing challenge. Complex graphene composites are increasingly reported, but the fate of pollutants and adsorption mechanisms are still far to be fully clarified. This review summarizes the recent progresses in the application of graphene-based adsorbents for eliminating a wide range of organic and inorganic pollutants from wastewater. A critical explanation is provided on the synthesis of graphene adsorbents, systematic adsorption and desorption mechanisms along with their pollutant removal performances under different experimental conditions. A brief perspective on upcoming research needs and challenges involved in the designing of high-quality graphene-based adsorbents are highlighted.

1. Introduction

Rapid increase in the world's population and continuous industrialization has made environmentalists more concerned about wastewater management. Different type of industries (*e.g.*, textiles, papers, fertilizer and agrochemicals, tannery) produces million tons of wastewater every day, and some of them are discharged into the surrounding water bodies without any primary or secondary treatments. This wastewater contains various inorganic (*e.g.*, heavy metals and earth rare metals) and organic pollutants (*e.g.*, dyes, pharmaceuticals, personal care products, PAHs, phenols, herbicides, pesticides) that are carcinogenic, persistent and bio-accumulative in nature [1–4]. Consequently, wastewater treatment is an urgent concern as it carries out detrimental impacts on human, animals, and the surrounding environment [5].

Several treatment technologies have been employed for the elimination of toxic pollutants from wastewater, such as adsorption, advanced oxidation process (AOPs), membrane separation, reverse osmosis, chemical precipitation, ion-exchange, electrochemical treatment, biological treatments [6–10]. Of all the treatment approaches, adsorption has been considered as the most promising one because of its high efficiency, ease of operation, cost-effectiveness and feasibility to implement at large-scale [11,12]. Moreover, it does not create any secondary pollution by generating toxic contaminants during the treatment

* Corresponding author at: State Environmental Protection Key Laboratory of Environmental Risk Assessment and Control on Chemical Process, East China University of Science and Technology, Shanghai 200237, China.
E-mail address: zhouyanbo@ecust.edu.cn (Y. Zhou).

https://doi.org/10.1016/j.cclet.2020.05.011
1001-8417/

process [13,14]. Throughout the recent years, researchers have been tested a variety of developed adsorbents, such as carbon nanotubes [15], activated carbons [16], clay minerals [17], polymers [18], agricultural wastes [19], zeolites [20] for the elimination of hazardous pollutants from aqueous solution. However, most of these adsorbents have been suffering from either low adsorption and desorption efficiency or lack the selectivity for target contaminants while removing the micro-pollutants from the aquatic environment [21].

Graphene, a two dimensional (2D) single layer sheet of carbon atoms organized in a sp^2-bonded honeycomb-like lattice structure has been emerged as a "wonder material" with a number of potential applications [22–24]. This newly discovered nanostructure has been considered as the thinnest material ever produced, and most likely the simplest form of carbon [25]. Since the discovery in 2004, graphene nanostructure has been successfully applied as the base materials in terms of basic research in many revolutionary fields due to its interesting mechanical and physicochemical properties, *i.e.*, large surface area, good thermal stability, high electrical conductivity, big aspect ratio, excellent mechanical strength, flexibility, and negligible thickness [26–28]. Recently, these exceptional properties have further expanded its application in environmental remediation as novel adsorbents for purifying wastewater [29,30]. It is very high theoretical surface area, abundant active sites and great delocalized π-electron systems made it superior adsorbent for capturing a wide range of both inorganic [31–33] and organic pollutants [34–36]. The polyaromatic π-electron system of graphene can interact with the aromatic structure of organic molecules *via* π-π interactions or strong hydrophobic effect, and merely remove them from aqueous solution [37].

The properties of pristine graphene have been improved by oxidizing it to graphene oxide (GO). The ample oxygenated functional groups of GO offer negative charges that significantly increase its hydrophilicity in aqueous solution and, thus, maximize the adsorptive interaction of GO with metal ions and positively charged organic pollutants [38]. Conversely, the reduction of GO forms reduced graphene oxide (RGO), contains carbon to oxygen ratio of 246:8 that made itself more advantageous than pristine graphene and GO in removing organic effluent from wastewater through π-π interactions [39]. Besides, surface modification of graphene, GO and RGO with specific functional groups, polymers or nanosized metal/metal oxides further accelerates their adsorptive interaction by generating additional functional groups, which favors in the selective elimination of various organic and inorganic pollutants [40,41]. Additionally, graphene adsorbents are less expensive in comparison to carbon nanotubes (CNTs) [42,43]. All these attractive features made graphene and their derivatives as ideal adsorbents for the elimination of numerous toxic pollutants from wastewater.

Research interest on graphene adsorbents is growing promptly, which is reflected by enormous research articles published throughout the last couple of years. There are some complex reviews exist in the literature concerning the synthesis and application of graphene adsorbents focusing either organic or inorganic pollutants, and in most of the cases lack the recent data [44,45]. Considering this, our review focuses on the systematic explanation of recent data regarding the use of graphene adsorbents in removing multiple categories of pollutants, *i.e.*, heavy metals, dyes, PAHs, antibiotics, phenols from wastewater, and represent the current research status. Nevertheless, synthesis and modification of graphene subsidiaries, their interaction mechanisms with aforementioned pollutants, applicable kinetic model along with experimental conditions, such as pH, temperature, contact time have been critically reviewed. Finally, some important clues in support of designing further better-quality graphene adsorbents are delivered.

2. Synthesis of graphene materials

Graphene subsidiaries can be existed in numerous forms, such as pristine graphene, GO and RGO. In addition, researchers have been developed a wide range of graphene composites materials in order to expand their application in environmental remediation [41].

2.1. Pristine graphene

Novoselov *et al.* [46] were the first who made a very stable and monocrystalline graphene sheet from pyrolytic graphite by mechanical exfoliation. Afterwards, several synthetic approaches have been manifested and applied to produce graphene, which can be classified into two major strategies *viz.*, "top-down strategy" and "bottom-up strategy" [47,48]. The top-down strategy refers to the separation of graphite layer into single or few layered graphene sheets by several exfoliation methods. Top-down strategies include mechanical exfoliation [46], chemical exfoliation [49], liquid-phase exfoliation [50], graphite intercalation compounds [51]. However, the best top-down strategy among them includes chemical exfoliation of graphite into graphite oxide using strong oxidizing agents and subsequently switches into graphene by chemical reduction or thermal exfoliation [52].

On the other hand, the bottom-up strategy is defined as the direct synthesis of graphene from carbonaceous gases or other hydrocarbon sources [53] by chemical vapor deposition (CVD) [54], epitaxial growth [55], template route [56] and substrate-free gas-phase synthesis (SFGP) [57]. Properties and application of fabricated graphene depend on their synthesis methods. Top-down strategy offers the large-scale production of graphene at low-cost, however, defects during the exfoliation process could deteriorate the quality of graphene sheets. In contrast, bottom-up strategy produces high-quality graphene sheets with exceptional properties, but the manufacturing cost is comparatively high [41]. The latest reviews by Lim *et al.* [52], Lee *et al.* [58] provide further details information about the synthesis routes of pristine graphene.

2.2. Graphene oxide (GO)

Graphene oxide (GO), a highly oxidative form of graphene obtains through either exfoliation or chemical oxidation of graphite flakes into discrete layers *via* sonication, mechanical stirring, rapid heating [59,60]. Usually, GO single layer is thicker than pristine graphene due to plenteous oxygen-containing functional groups, present on both sides of GO layer (*e.g.*, hydroxyl (−OH) and epoxy (C—O—C) groups on the basal plane, and carboxyl (−COOH) and carbonyl (–C = O) groups at the sheet edges) [61,62]. These oxygen-containing functional groups are more crucial in adsorption, which determines the binding ability of GO to pollutants. The extent of oxygenated functional group generates on GO surface relies on both the nature of its precursor graphite materials [63] and the degree of oxidation level [64].

A number of synthesis methods have been reported to produce GO between the years of 1859 and 1958, mostly include Brodie method ($KClO_4$, HNO_3) [65], Staudenmaier method (H_2SO_4, $KClO_4$, HNO_3) [66] and Hummers' method (H_2SO_4, $NaNO_3$, $KMnO_4$) [67], which are comprise the primary pathways of synthesizing GO [44]. Of them, Hummers' method has gained the highest attention as the most well-known and adopted method in adsorption. Afterwards, some significant changes have been implemented to Hummers' method in order to enhance the degree and range of functionalities on GO surface as well as to reduce the release of toxic gases [42]. In the Hummers' method, a mixture of (1:3, wt equiv.) $NaNO_3$ and $KMnO_4$ along with H_2SO_4 (69 mL) were added to 3 g (1 wt equiv.) of

graphite flakes [67]. In contrast, modified Hummers' method has some differences in the mixture ratio of $KMnO_4$ and graphite flakes [68], and in most cases $K_2Cr_2O_7$ is used instead of $KMnO_4$ as described by Upadhyay *et al.* [69]. Marcano *et al.* [68] presented an improved version of Hummers' method by using a 9:1 mixture of concentrated H_2SO_4/H_3PO_4 (360:40, mL:mL) without $NaNO_3$ and achieved the equivalent product like conventional Hummers' method. The key advantages of this method include the production of highly oxidized GO with low-cost than reported by Hummers' and modified Hummers' method, and does not create toxic gas like NO_x. Fig. 1 demonstrated the detail comparisons of these methods. Improved Hummers' methods have been further thoroughly investigated by Yadav *et al.* [70], Sohail *et al.* [71], Chen *et al.* [72].

2.3. Reduced graphene oxide (RGO)

Reduced graphene oxide (RGO) is another important derivative of the graphene family. Due to reduced form, it contains a smaller quantity of residual oxygenated functional groups, therefore, less negatively charged than GO. RGO can be synthesized by following two major routes, *i.e.*, the direct growth and the chemical/thermal reduction of GO (Fig. 2) [61]. In general, the chemical reduction of GO is widely employed in adsorption practices due to its cost-effectiveness, and high throughput.

A large number of reductants have been experienced in the reduction of GO such as hydrazine hydrate, vitamin C, alcohols, $NaBH_4$, NaOH, KOH, HI, Zn and $Na_2S_2O_3$ [61]. The removal of oxygen moieties from GO surface is a vital issue that determines the properties of RGO. In case of deoxygenation, hydrazine hydrate is much more efficient than other reductants like $NaBH_4$ because of its high potentiality in reducing the majority of oxygen-containing functional groups *via* a direct nucleophilic attack. The continuous accumulation of nitrogen atoms from hydrazine leads to the formation of C—N groups through the breaking down of oxygenated functional groups. Usually, hydrazine reduction is known to form hydrocarbons, while $NaBH_4$ reduction forms residual hydroxyl functional groups. Consequently, hydrazine is expected to be a better reducing agent than $NaBH_4$ for GO [73]. Table S1 (Supporting information) compared the reduction degree of several reductants, where hydrazine hydrate demonstrated the highest value of C/O ratio with improved electrical conductivity for RGO. With the deduction of bulk oxygen moieties, the resultant RGO exhibited high hydrophobicity with the significant restoration of sp^2 carbon structure [74]. However, excessive use of aforesaid reducing chemicals can contaminate the RGO by incorporating harmful impurities, which might cause damaging effects on the environment [75]. These toxic chemicals can be replaced by the use of eco-friendly green reducing agents, such as, tea solution, reducing sugars, tamarind extract, eucalyptus leaf extract, carrot root, green tea [76]. Green synthesized RGO also exhibits improved adsorption capacity to diverse pollutants, which is now an ongoing research trend in adsorption studies [75,77].

Another facile route to prepare high-quality RGO, termed as PG, using H_2 plasma was reported by Wang *et al.* [78]. First, GO was pickled in a home-made plasma generator incited by a radio frequency inductively coupled plasma. After reducing the pressure to 3 Pa, pure H_2 was added to reactor *via* a gas mass flow controller at a flow rate of 30 cm^3/min. After that, the H_2 plasma going on at 10 Pa was functioned for 30 min to covert GO into RGO. Further detail information on the synthesis of RGO can be explored from the comprehensive review by Singh *et al.* [57], and Krishnan *et al.* [79].

2.4. Graphene based composites

The potentiality of graphene adsorbents largely depends on their uniform dispersion in solution along with high sorption capacity to diverse pollutants. Usually, graphene shows high affinity to aggregate or even rolls to form graphite during liquid processing. The resulting aggregation can limit its adsorptive application by blocking active sorption sites; decreasing theoretical surface area as well as by hindering rapid mass transport [60,80]. In case of GO, it shows poor binding affinity to anionic dyes owing to electrostatic repulsion between them. In addition, because of high solubility, GO cannot easily be regenerated from treating wastewater [41]. All these shortcomings can be overwhelmed through various covalent or non-covalent functionalization with dissimilar molecules, polymers and nanoparticles, thus, developing composites, a class of multicomponent materials, is investigated [81]. The resulting composite is not merely the sum of the individual components, but instead a new material with new functionalities and properties [41]. Table 1 [82–99] summarizes the recent works in the development of graphene composites materials.

2.4.1. Graphene polymer composites

Polymeric modifications of graphene not only enhance the possibility of attaching new functional groups on graphene surface but also increase the number of active sites to fix numerous organic and inorganic pollutants [40]. Based on 3D arrangements and the mode of interaction between graphene sheet and polymer, graphene polymer composites can be classified into three types: (1) layered graphene-polymer films, (2) graphene-filled polymer composites, (3) polymer-functionalized graphene nanolayers [81]. The quality of graphene filler and polymer matrix, graphene dispersibility, filler and matrix bonding, ratio of filler to matrix

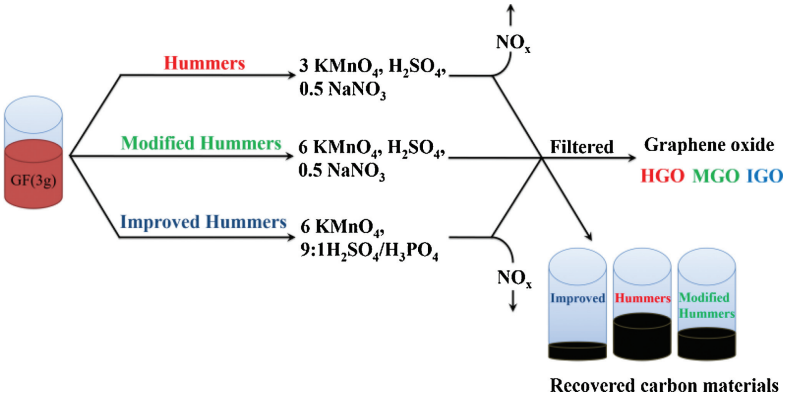

Fig. 1. Comparative synthesis routes of GO from graphite flakes by Hummers', modified Hummers' and improved Hummers' methods. Reproduced with permission [68]. Copyright 2010, American Chemical Society. The numbers mentioned in the figure are their weight equivalent clarified in the description.

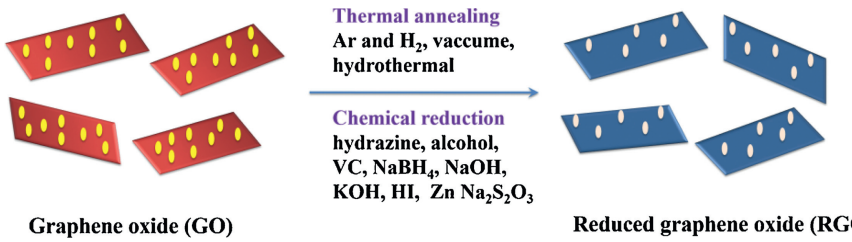

Fig. 2. Synthesis of RGO through chemical and thermal reduction. Reproduced with permission [61]. Copyright 2016, Elsevier.

Table 1
Synthesis of graphene composites with their respective adsorbates.

Graphene composite materials	Preparation methods	Specific surface area (m^2/g)	Adsorbates	References
Fe_3O_4@GO	Co-precipitation	167.9	Cu(II)	[82]
GO–carbon composite	Sol-gel method	174.3	Hg(II)	[83]
GO–$ZrO(OH)_2$	Hydrothermal co-precipitation method	266.9	As(III) & As(V)	[84]
Polyamide-graphene	Interfacial polymerization	421	Sb(III)	[85]
Fe_3O_4–RGO–MnO_2	Co-precipitation	113.7	As(III) & As(V)	[86]
GO/bentonite	Modified Hummers' method	63.4	Toluidine blue	[87]
Fe_3O_4@GO-thiourea	Solvothermal method	56.267	Coomassie brilliant blue	[88]
GO-magnetic iron oxide	Sonochemical method	84.63	Methyl blue	[89]
GO-polystyrene	Polymerization	9.5262	Reactive blue, Direct red	[90]
PDA-RGO-kaolin	Polymerization method	35.35	Methyl blue	[91]
Magnetic-$CoFe_2O_4$/GO	Hydrothermal method	27.30	Methylene blue, Rhodamine B	[92]
GO-montmorillonite	Solvent method	110.47	Crystal violet	[93]
Hollow carbon spheres/graphene	Hydrothermal method	356.1	Methyl orange, Rhodamine B	[94]
Graphene-CNT	Modified Hummers' method	78.9	Methyl blue	[95]
RGO/iron oxide composites	Co-precipitation	272.5	Naphthalene, 1-Naphthol	[96]
Graphene-MOF	Crystallization	2390	Benzene	[97]
Fe_3O_4 grafted GO	Co-precipitation	148.8	2,4,4-Trichlo-robiphenyl (PCB 28)	[98]
Graphene/MnO_2	*In situ* hydrothermal method	106	Tetracycline	[99]

could significantly alter the properties of graphene polymer composites [100]. Generally, the consistency between pristine graphene and organic polymers is very poor [101]. In contrast, GO and RGO are more compatible with organic polymers and attracted considerable attention as nanofiller to form polymer composites. The van der Waals interactions between GO layers can be altered significantly by the presence of oxygen-containing functional groups and improve its hydrophilicity in water. Thus, GO exhibits high solubility and, thereby, merging affinity with hydrophilic polymers, resulting in the formation of polymer composites with high mechanical and thermal stability [102]. There are several methods of incorporating polymers into the graphene matrices, *i.e.*, *in situ* polymerization, covalent bonding, solution (or solvent) mixing and melt compounding, *etc.* A detail explanation of these methods was summarized by Phiri *et al.* [100] and Itapu *et al.* [102]. However, it is crucial to know the interaction dependence of polymers and graphene on hydrophobicity, reactivity, polarity, molar mass, *etc.* during the selection of preparation routes [100].

Throughout the recent years, plenty of graphene polymer composites were synthesized and employed for adsorptive remediation of many pollutants. Majority of these were fabricated using GO and RGO as the fillers, which are based on polymers range like polyurethane [103], polyoxyethylene [104], polyethylenimine (PEI) [105], poly(ethylene glycol) diacrylate [106], poly-diallyldimethyl ammonium chloride [107], poly(*N*-vinylcarbazole) [108], *etc.* All these developed composites demonstrated better sorption efficiency than the individual polymers and graphene.

2.4.2. Graphene nanoparticle composites

Nanoparticles that are range from a few nanometers to a hundred nanometers in diameter can be adorned on graphene, GO and RGO, resulting in the formation of graphene nanoparticle composites. They can be categorized as (1) graphene-nanoparticle composites, where the nanoparticles decorate or are grown on graphene sheets, or (2) graphene-encapsulated nanoparticles, where the nanoparticle surface is wrapped or coated with graphene [109]. The existence of oxygenated functional groups and defects on the surface of graphene, GO and RGO provide them an excellent platform for the nucleation, growth, and attachment of various metals, such as Ag [110,111], Cu [112,113], Fe [114–116], Co [117,118], Ni [119–121], and metal oxide nanoparticles, such as TiO_2 [122,123], Fe_3O_4 [124,125], SiO_2 [126,127], MnO_2 [128,129], Al_2O_3 [130], CuO [131] As a consequence of the synergistic effect between graphene and the firmly fixed nanoparticles, these composites showed enhanced adsorption properties to a variety of pollutants. Several approaches have been reported for the development of graphene nanoparticle composites, such as sol-gel method, hydrothermal/solvothermal method, self-assembly, *in situ* growth strategy, electrochemical deposition, and microwave irradiation [109,132].

3. Application of graphene materials in adsorption

3.1. Adsorption of inorganic pollutants

Among the inorganic pollutants occur in wastewater, heavy metals (Pb, Cd, Hg, Ni, Cu, Zn, Cr, Sb, Cd, Co, Mn, *etc.*) and rare metals (Eu, Gd, La, Nd, Yb, *etc.*) are the most predominate because of their high toxicity to plants, animals, and human beings [133–135]. Heavy metals are bio-accumulative and cannot easily be degraded by chemical degradation or bioprocess [136]. Adsorption is proven to be the most effective technique in removal of metal ions from solution [137,138]. Graphene adsorbents have been widely acknowledged for the high removal of metal ions because of

their superior adsorption capacity. The recent progress in the adsorption of metal ions by graphene adsorbents are presented in Table 2 [33,139–157] .

Adsorption process could be driven through various interactions, such as electrostatic interactions, ion exchange, and surface complexation between metal ions and numerous functional groups present on the surface of graphene adsorbents [61, 158,159]. Sitko *et al.* [160] reported that metal ions can be adsorbed on the surface of GO nanosheets through chemical adsorption, which involves strong electrostatic interactions between positively charged metal ions and negatively charged GO sheets. Ion exchange is another important mechanism that occurs between metal ions and protons (H^+ ions) from −COOH or −OH oxygenated functional groups. During the adsorption process, H^+ ions from −COOH or −OH are released to the solution, leading to lower the pH than the initial value. For example, the exchange of Pb(II) and H^+ was the crucial mechanism for adsorptive removal of Pb(II) from aqueous solution reported by Madadrang *et al.* [161]. Besides, surface complexation between metal ions and oxygen-containing functional groups of graphene are evidenced to play a significant role in the adsorption of Pb(II). The Pb(II) made complexation with ionized −OH group of "free" hydroxyl groups and bonded −OH bands of carboxylic acids [63].

However, several experimental parameters, such as temperature, pH, contact time, adsorbent dose, foreign ions, and ionic strength can significantly affect the adsorption mechanism of metal ions [44,61]. Solution pH should be adjusted carefully during the adsorption process as it could significantly affect the surface charge of adsorbents and ionic species of metal [162]. At low pH, high concentration of H^+ and H_3O^+ in solution could compete with metal ions to attach with available binding sites of graphene surface. Alternatively, oxygenated functional groups present on the surface of graphene adsorbents are deprotonated at high pH, offering more ligands to bind metal ions [61]. Usually, metal ion species are present in aqueous media in the form of M^{n+}, $M(OH)_n$, $M(OH)^+_{n-1}$, $M(OH)^-_{n+1}$ and $M(OH)^{2-}_{n+2}$ at different pH range due to the hydrolysis reactions. At high pH, $M(OH)^-_{n+1}$ and $M(OH)^{2-}_{n+2}$ are dominant species, resulting in electrostatic repulsion with the negatively charged oxygenated functional groups, thus, reduce the sorption capacity. Consequently, the optimum pH range for metal adsorption may be different due to their dissimilarities in the metal electronegativity and the first stable constant of related metal hydroxides [44].

Temperature may affect the adsorption of metal ions by alternating the solubility and molecular interactions with solid particles. Increasing temperature may lead to the increase either the extent of sorption sites on the surface of graphene adsorbents or the rate of metal ion diffusion from solution to the graphene surfaces, thereby, increasing the adsorption rate [163]. The presence of foreign ions in solution would compete with metal ions for limited active sites on solid particle surfaces, which ultimately reduces the adsorption capacity. Besides, ionic strength could remarkably influence the electrostatic interactions, which would then impact the particle aggregation. Activity coefficients of metal ions also could be affected by ionic strength, thus, limits the metal ions diffusion from the solution to the adsorbent surface [164].

For the removal of metal ions, GO is more preferred than RGO due to abundant oxygen-containing functional groups, which can easily bind the positively charged metal ions through electrostatic attraction. For example, Li *et al.* [165] compared the adsorption capacity of U(VI) using GO and RGO where they found GO was much more efficient than RGO due to the presence of oxygen-containing functional groups. Zhao *et al.* [166] further confirmed that the oxygen-containing functional groups were the key factor for the adsorption of U(VI). However, adsorption performances of GO to metal ions may vary according to its precursor graphite materials, which ultimately define the amount of oxygen-containing functional groups generate on GO surface. For instance, GO synthesized from amorphous graphite showed better adsorption capacity (766.8 mg/g) than produced by flaky graphite (746.2 mg/g) and lump graphite (738.5 mg/g) [63].

Reynosa-Martínez *et al.* [64] evaluated the adsorption capacity of GO nanosheets according to their degree of oxidation levels. The maximum adsorption capacity of As(III) raised from 123 mg/g to 288 mg/g, with the oxidation level increased from 1.98 C/O to 1.35 C/O ratios using $KMnO_4$. The elevated sorption capacity was attributed to the enhanced oxygen-containing functional groups generated as a result of high oxidation level evident by FT-IR spectra of GO. In a recent study, Kong *et al.* [167] showed that adsorption performance not only depends on the properties of GO but also on the characteristics of metal ions *i.e.*, atomic number,

Table 2
Adsorption of metal ions from aqueous solution by different graphene adsorbents.

Graphene adsorbents	Adsorbates	Experimental condition				Maximum adsorption capacity, Q (mg/g)	References
		Conc. (mg/L)	pH	Temp. (K)	Time (h)		
Graphene QDT@$NiFe_2O_4$-HNT	Pb(II)	10-100	6.0	298	0.83	42.02	[139]
GO/alginate hydrogel	Pb(II)	5–40	5.0	303	24	327.9	[140]
Glycol-GO	Pb(II)	100	2.0-6.0	298	48	146	[141]
Polyethylenimine- GO-polystyrene	Pb(II)	50	6.0	303	0.16	290	[142]
Magnetic GO/hydrogel	Pb(II)	20–200	2.0–6.0	293	24	81.78	[143]
Fe_2O_3-graphene aerogel	As(V)	5–70	2.0–12.0	298	4	217.34	[144]
GO/$MnFe_2O_4$	As(V)	0–50	1.0–2.0	298	1.5	240.4	[145]
Graphene aerogels	Cd(II)	25–200	8.0	298	2	149.25	[146]
Polyethylenimine- GO-polystyrene	Cd(II)	50	8.0	303	0.25	180	[142]
GO-OCH_2COOH	Cu(II)	100	6.0	298	24	93.8	[33]
Magnetic GO-hydrogel	Cu(II)	20–200	2.0–8.0	293	24	69.67	[143]
Fe_3O_4/GO/DCTA	Cu(II)	0.001	8.0	303	24	74.05	[147]
RGO-montmorillote	Ni(II)	100	7.0	303	120	625	[148]
Fe_3O_4/graphene	Cr(VI)	75–600	3.0–4.0	298	24	280.6	[149]
Graphene coated iron oxide	Cr(VI)	–	2.0	323	0.5	352.1	[150]
3D CD@RGO	Hg(II)	0.2–10	7.0	298	12	82.64	[151]
Xanthate magnetic-GO	Hg(II)	20	7.0	–	3	118.55	[152]
GO/CMC monoliths	Co(II)	40–120	–	298	–	59.99	[153]
Magnetic-chitosan/GO	Pb(II)	–	5.0	303	1	76.94	[154]
RGO/$CoFe_2O_4$/polyaniline	U(VI)	50	5.0	298	–	2430	[155]
GO/bentonite	U(VI)	400	7.0	303	0.2	234.19	[156]
Chitosan/GO	Au(III)	80–500	–	298	16	1076.649	[157]

ionic radius, electronegativity, atomic weight, covalent index, atomic radius, softness index, *etc.* Based on aforementioned characteristics, they explored the adsorption performance of GO towards metallic hard (Na, Mg), soft (Cd and Pb) and borderline ions (Ni, Cu, Zn, Co), and reported that removal rate of hard ions was substantially lower than that of soft and borderline ones.

Surface modification of GO and RGO with different organic and inorganic entities introduces additional functional groups that extensively enhance their metal sorption sites. Zhu *et al.* [168] investigated the adsorption performance of brianyoungite-graphene oxide (BY-GO) composites for Cu(II) in solution. The maximum adsorption capacity achieved 1724.1 mg/g, which was much higher than individual GO and BY. The high removal rate was attributed to the enhanced oxygen-containing functional groups on BY-GO composites, which tends to bind Cu(II) through Cu-O coordination. The adsorption scheme of Cu(II) onto BY-GO composites was visualized in Fig. 3. The adsorption capacity was reported to be increased with increasing pH, obtaining a maximum at pH 5.23. Above this point, the formation of $Cu(OH)_2$ causes the decrease of Cu(II), which leads to decrease the adsorption.

Amorphous magnetic-GO/RGO nanocomposites have received enormous attention for metal adsorption, especially for arsenic, because of their large specific surface area and better dispersibility in water [169,170]. Zhang *et al.* [171] described high removal rate of 160.65 mg/g and 104.13 mg/g for As(III) and As(V) ions, respectively, by ionic liquid assisted magnetic-GO (MGO-IL) nanocomposites, which was far greater than shown by other graphene adsorbents, such as GO-$ZrO(OH)_2$ [84] and Fe_3O_4-GO-MnO_2 composites [172]. Removal mechanisms were found to be varied over a wide pH range. At low pH, As(III) and As(VI) were isolated *via* electrostatic attraction, whereas, at high pH, As(III) occurred in the form of $As(OH)_3$, resulting in the formation of As-O-Fe bonding *via* surface complexation.

However, Yoon *et al.* [173] reported that MGO is more effective in removal of both As(III) and As(VI) metal ions than that of MRGO composites because of more functional groups. Nevertheless, the increased adsorption capacity of MGO nanocomposites was noted with increasing the amount of iron-oxide loading to filler GO due to enhanced active sites. For example, Su *et al.* [174] compared the adsorption rate of As(III) and As(V) onto FeOx-GO nanocomposites having different iron oxide content (36–80 wt%). Among the developed composites, FeOx–GO-80 (80 wt%) displayed the highest sorption capacity of 147 mg/g and 113 mg/g for As(III) and As(V), respectively, whereas, FeOx–GO-36 (36 wt%) exhibited 19 mg/g and 59 mg/g.

Silicon dioxide (SiO_2), an excellent coating material with several traits like hydrophilicity, negative charge, shows outstanding metal sorption capacity when coated on GO surface. Adsorption of Pb(II) and As(III) metal ions by IL-assisted mesoporous GO/SiO_2 composites have been studied by Barik *et al.* [175]. The maximum adsorption capacity was achieved 527 mg/g and 30 mg/g for Pb(II) and As(III) ions, respectively. The experimental data were fitted well with the *pseudo*-second order kinetic model for both Pb(II) and As(III). On the contrary, Langmuir model was more suitable for Pb(II), whereas, the Freundlich model for As(III) adsorption process. In another study, Molaei *et al.* [176] prepared a novel sandwich-like GO@SiO_2@C@Ni composites under temperatures ranges from 400 °C to700 °C, and applied for the removal Cr(VI). Ni was chosen as the "captured" metal-ions because it possesses high stability, some reducibility and bigger magnetic intensity under low temperature. The results revealed that GO@SiO_2@C@Ni-400 composites shown the highest removal capacity for Cr(VI) than GO@SiO_2@C@Ni-700, because of enormous functional groups, larger surface area and incomplete combustion of Ni. The high temperature leads to decompose most of the oxygenated functional groups and Ni particles, thereby, decreases the oxygen contents favorable for Cr(VI) adsorption.

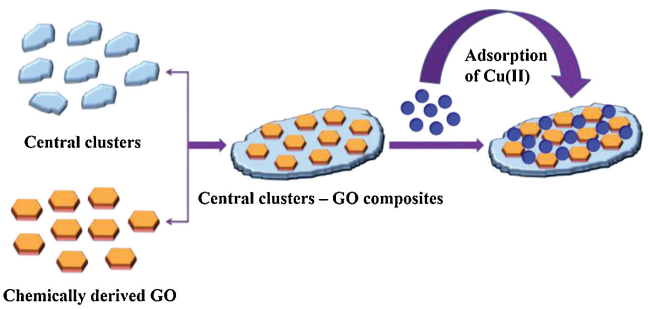

Fig. 3. Adsorption of Cu(II) on BY-GO composites. Reproduced with permission [168]. Copyright 2016, American Chemical Society.

Compared with inorganic composites, organic polymer composites are more effective for adsorptive removal of metal ions as they possess chelating groups, which are selective and favorable to bind metal ions [44]. Moreover, some polymers, such as polyaniline, polyethylenimine and polypyrrole possess nitrogen-containing functional groups that provide further excellent adsorption/complexing sites for metal ions [177]. Zhou *et al.* [178] reported high removal of Hg(II) from aqueous solution by magnetic polypyrrole-graphene oxide (MPPy-GO) composites. The maximum removal rate of Hg(II) by MPPy-GO composites was recorded 400.0 mg/g at 300 K and pH 7 ± 0.1. The FT-IR data and zeta potential indicated that the magnitude of negative charges on MPPy-GO composites increased radically with increasing solution pH, which attracted the positively charged Hg(II) *via* electrostatic attraction. Similarly, Xing *et al.* [179] reported that adsorption capacity of poly(allylamine hydrochloride)-GO (PAH-GO) composites for Cu(II) increasing with pH value 1.0–6.0. The maximum adsorption capacity was about 349.03 mg/g at 293 K and pH 6.0. At high pH, the surface complexation between amino groups of PAH and Cu(II) rises, which results in an increased elimination rate of Cu (II) ions from solution.

Chitosan (CS) is another important biopolymer that can easily combine with graphene derivatives to form chitosan-graphene composites with excellent properties and enhanced metal sorption capacity [180,181]. Sharma *et al.* [182] reported a high selective removal capacity of cross-linked chitosan grafted on aminopropylsilane-GO (CS-APS-GO) composites for Pb(II). The maximum adsorption capacity of CS-APS-GO was achieved 566.2 mg/g at pH 5.0. The cross-linked CS-APS-GO composites had been decorated with active adsorption sites (*e.g.*, $-NH_2$/=NH) with lone pair(s) of electron. The substantial propensity for lone pair electron donation played a crucial role for the binding of metal ion in the formation of metal complexes. In the same way, Samuel *et al.* [183] studied the adsorption capacity of chitosan-GO (GO-CS) composites for the adsorptive removal of Cr(VI) within the pH range of 1.0–11.0. The maximum adsorption capacity of Cr(VI) was recorded 104.16 mg/g at pH 2.0. The quantity of Cr(VI) adsorbed on GO-CS composites found to be increased with respect to an increase in contact time and reached at equilibrium within 420 min.

3.2. Adsorption of organic pollutants

3.2.1. Adsorption of dyes

Textile, dyeing, printing, ink, and related industries continuously generate a large volume of effluent that contains colored dyes and pigments. These organic compounds are highly resistant to degradation because of their complex chemical structures, and pose a serious threat to human and environment, even at very low concentrations [184,185]. Dye pollutants are highly dissolved in water and can be categorized as either cationic or anionic ions, and

few are dispersive [101]. Graphene and its derivatives show outstanding adsorption performances to a variety of dye molecules, because of plausible adsorptive interactions happen between them.

Electrostatic interaction between graphene and dyes is considered as the most significant mechanism for adsorptive removal of dye molecules. As mentioned earlier, GO contains abundant oxygen-containing functional groups that hold negative charge, can easily bind with positively charged cationic dyes through electrostatic attraction [186]. Peng *et al.* [187] reported a high removal rate (2255.35 mg/g) of methylene blue (MB) by GO due to strong electrostatic attraction between them. The adsorption rate was found to be high at pH 5.0–12.0 because of negative zeta potential of GO. Bradder *et al.* [188] examined the adsorption capacity of MB and malachite green (MG) onto GO and reported the Langmuir adsorption capacity of 350 mg/g and 248 mg/g, respectively. The authors also identified the electrostatic attraction between oxygenated functional group of GO and positively charged dye molecules was responsible for such greater adsorption.

Nevertheless, as like metal ions, adsorption performances of GO to dyes could be varied depending on the degree of oxidation level. Thangavel *et al.* [189] synthesized GO sheets with various oxidation levels and compared their adsorption performances to MB. Highly oxidized GO displayed upmost adsorption capacity, which then decreased gradually with oxidation level as GO1−99.8 mg/g > GO2−97 mg/g > GO3−95 mg/g > GO4−90 mg/g. This variation was due to the extent of oxygenated functional groups generated on the GO surface during the oxidation process. When the degree of oxidation level increased, more functional groups was attached to the basal plane of GO, which resulted more adsorption sites for MB.

However, due to electrostatic repulsion, GO nanosheets are not favorable for the removal of anionic dyes from solution. Konicki *et al.* [190] studied the adsorption capacity of GO towards anionic azo-dyes, such as acid orange 8 (AO8) and direct red 23 (DR23). When the initial pH of the dye solution increased from 3.0–11.0, electrostatic repulsion between oxygenated group of GO and sulfonate anions ($R\text{-}SO_3^-$) of azo dyes was found to be too strong to decrease the adsorption capacity from 27.8 mg/g to 11.2 mg/g and 23.3 mg/g to 8.5 mg/g for AO8 and DR23, respectively.

In that case, GO could be reduced or modified with polymers or nanoparticles, contain $–NH_2$ groups in order to introduce positive charge on GO surface [186]. For example, Ramesha *et al.* [191] converted GO into RGO and reported increased removal efficiency of RGO (from 50% to 95%) for anionic dyes. The presence of lot of defects, residual oxygen functionalities, wrinkles and π-electron domains in the lamellar structure of RGO, made it an ideal adsorbent for both cationic and anionic dyes [41]. Residual oxygen functionalities play dominant role during the adsorption of cationic dyes *via* electrostatic interaction, whereas, wrinkles and π-electrons for both cationic and anionic dyes through pore-filling diffusion and π-π interaction, respectively [192]. It is worth mentioning that π-π interaction is another leading dye removal mechanism that happens between delocalized π-electrons of graphene and aromatic rings of dyes [193].

RGO prepared by the reduction of fine fraction of GO showed excellent sorption capacity (476.2 mg/g) for malachite green (MG) [194]. The presence of several wrinkles, bends, and folds owing to structural defects were explicitly observed in the RGO surface marked by HRTEM images. The average pore diameter for RGO was estimated to be 2.96 nm using BJH model, with the pore size distribution focused in the micropore and mesopore range. This lamellar structure with nanoscale wrinkles, bends and folds provides ample avenues for diffusion of MG into micropores and groove region of wrinkles *via* pore-filling mechanism. Moreover, the π-π interaction between the graphitic skeleton of RGO and aromatic rings of MG, along with electrostatic interaction between cationic center of MG and residual oxygen functionalities of RGO (at neutral and alkaline pH) jointly facilitate the adsorption of MG onto RGO. The adsorption process was reported endothermic and spontaneous.

Reducing agents spent during the reduction of RGO could significantly affect the adsorption performances of dyes. For example, Sykam *et al.* [195] represent a rapid and efficient large-scale green reduction method of RGO from GO using Tulasi (Holy Basil) green tea extract and reported greater sorption capacity of 416.7 mg/g for MG at high pH following Langmuir and *pseudo*-second order kinetic models. In the same way, Rajumon *et al.* [76] also synthesized RGO by green reducing agents *Tamarindus indica* and applied for adsorptive removal of MB and basic fuchsin (BF). From the Langmuir isotherm model, the maximum adsorption capacity was noticed to be 238.09 mg/g and 243.90 mg/g, respectively for MB and BF. Xiao *et al.* [196] designed L-cysteine reduced GO (RGO-Cys) for the adsorptive removal of indigo carmine (IC) and neutral red (NR) from aqueous solution. Owing to strong π-π interaction between the substrate of graphene and organic dyes, the maximum adsorption capacity of IC and NR were as high as 1005.7 mg/g and 1301.8 mg/g, respectively.

Composites of graphene show enhanced removal performances by introducing supplementary functional groups, which may generate new adsorptive interaction with dye molecules *i.e.*, hydrophobic interaction, H-bonding, van der Waals interaction, Lewis acid-base interaction, *etc.* For instance, Das *et al.* [197] fabricated Gd_2O_3/Bi_2O_3@GO composites and applied to remove methyl orange (MO) from aqueous solution. The maximum adsorption capacity was recorded as 544 mg/g, which was comparatively higher than individual Bi_2O_3@GO (308 mg/g) and Gd_2O_3@GO (392 mg/g). The H-bonding between oxygenated functional groups of Gd_2O_3/Bi_2O_3@GO and nitrogen-containing group of MO was specified as the principal adsorption mechanism. Fig. 4 illustrated the formation of H-bonding between Gd_2O_3/Bi_2O_3@GO and MO.

Heidarizad *et al.* [198] reported a high removal rate of MB by GO/MgO composites. Due to strong electrostatic interactions, the composites showed high adsorption capacity as 833 mg/g at high pH, which was comparatively higher than pure GO and MgO. Tan

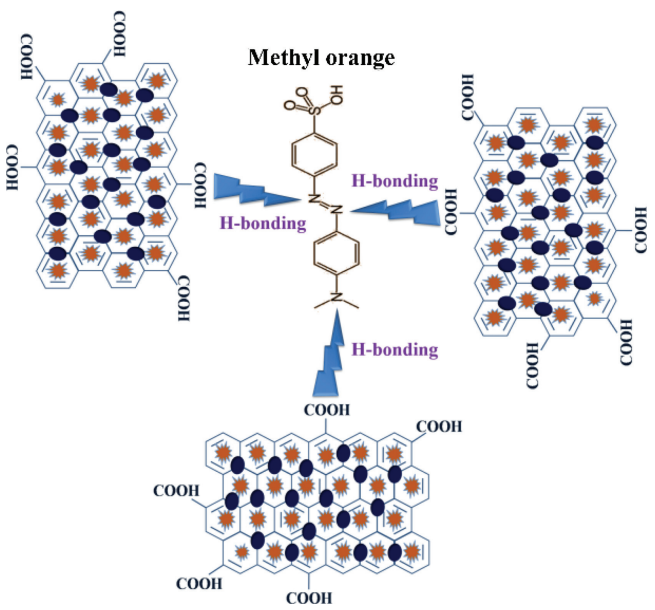

Fig. 4. Bonding mechanism of Gd_2O_3/Bi_2O_3@GO with MO. Reproduced with permission [197]. Copyright 2016, Elsevier.

et al. [199] synthesized graphene/beta-cyclodextrin (GNS/β-CD) composites and employed to remove MB, MO and BF from water. The maximum adsorption capacities for MB, MO and BF onto GNS/β-CD composites were 580.4, 328.2 and 425.8 mg/g, respectively. Due to the less oxygen-containing groups on composite surface, π-π interaction was claimed to be responsible for high adsorption rate.

Montmorillonite (Mt)-GO/RGO composites have gained tremendous attraction for higher removal of various dye molecules because of unique properties, such as strong cation exchange capacity, large surface area as well as the synergistic effects between Mt and GO/RGO. Moreover, Mt clay minerals holding a net negative charge that can be easily exploited to specifically adsorb positively charged pollutants. Puri *et al.* [93] formulated GO/Mt nanocomposites and reported very high removal rate of 746.27 mg/g for crystal violet (CV) dyes in water. The data obeyed Langmuir and *pseudo*-second order reaction models. The high adsorption capacity was attributed to π-π interactions and H-bonding between composites and CV.

Yang *et al.* [200] compared the adsorption capacity of GO/Mt and RGO/Mt for MB and demonstrated that GO/Mt showed greater removal capacity (486.2 mg/g) than that of RGO/Mt (478.3 mg/g), because of high oxygen-containing functional groups. In another study, Neelaveni *et al.* [148] synthesized GO/Mt composites with different ratios of Mt to GO (5:1, 10:1, 15:1 and 20:1) and applied for the deletion of Rhodamine B (RhB) in solution. Among them, GO/Mt composites with (1:10) ratio showed the highest uptake (625 mg/g) of RhB at neutral pH condition. Authors stated that the low adsorption efficiency of the composites with higher ratio, may be due to agglomeration of Mt on GO.

Polymers that hold nitrogen-containing functional groups show greater adsorption capacity for wide range of dyes (especially for anionic dyes) when embedded on graphene surface. The lone pair of electrons in several nitrogen-containing functional groups (*e.g.*, amino, imine, amidoxime, imidazole and hydrazine groups) provide strong coordination aptitude with multifarious dye pollutants [201]. Besides, these functional groups can easily be protonated under acidic environment, thus, offering high selectivity towards anionic dye molecules *via* strong electrostatic attraction [202].

For example, GO was functionalized with poly(*N*,*N*-dimethyl amino ethylmethacrylate) (PDMAEMA) and employed for the selective removal of orange G (OG) [203]. After functionalization, zeta potential of GO-PDMAEMA was changed from negative (GO for -36.5) to positive (41.5), which made it an effective adsorbent for anionic OG. The maximum adsorption capacity was recorded as 609.8 mg/g with electrostatic attraction as the key driving force between anionic OG and positively charged GO-PEMAEMA, which was further confirmed by the competitive effect of salt concentration (Cl^- and SO_4^{2-}) on OG adsorption. Selectivity of GO-PEMAEMA was tested with a mixture of cationic MB and anionic dyes (OG, EY and CR) under the same concentration. According to the UV-vis spectra, the characteristic peaks of OG (at 478 nm) and EY (at 518 nm) were decreased significantly after adsorption whereas, the change for MB (662 nm) is very limited, which indicate that electrostatic attraction between anionic dyes (OG or EY) and positively charged GO-PDMAEMA is mainly responsible for the selective adsorption of anionic dyes from their mixture.

Ansari *et al.* [204] prepared polyaniline modified multiwalled carbon nanotube-GO (GO-CNT) composites doped with *para* toluene sulphonic acid (pTSA). The resulting pTSA-Pani@GO-CNT was utilized for removing congo red (CR) from aqueous solution. The functional groups present on pTSA-Pani@GO-CNT, such as amine, hydroxyl, and carboxyl were protonated under acidic condition and generated a positive charge on the adsorbents, which strongly attached with anionic CR through electrostatic attraction. The highest removal rate of CR (66.66 mg/g) was observed in acidic medium followed by *pseudo*-second order kinetics and Langmuir isotherm models. With the increasing solution pH, deprotonation of functional groups initiated and a negative charge aroused on adsorbent surfaces, which repelled the anionic CR and decreased the adsorption rate.

Recently, 3D graphene-derived structures, such as foams [205], sponges [206], aerogels [207] and hydrogels [208], all displayed outstanding adsorption performances to dye molecules. The inherent features of 3D graphene structure, such as large specific surface area, multi-level pores including micropore, mesopore, and macropore offer plenteous active sorption sites for trapping different dye pollutants [209]. Zeolitic imidazolate framework-

Table 3
Adsorption of dyes from aqueous solution by different graphene adsorbents.

Graphene adsorbents	Adsorbates	Experimental condition				Maximum adsorption capacity, Q (mg/g)	References
		Conc. (mg/L)	pH	Temp. (K)	Time (h)		
Silk fibroin@GO	Methylene blue	50–200	7.0	303	120	1322.71	[212]
GO-activated carbon	Methylene blue	40–100	3.0	298	1.5	147	[213]
Sodium dodecyl sulfate/graphene	Methylene blue	10–100	3–9	298	48	782.3	[214]
GO/$MnFe_2O_4$	Methylene blue	2–8	7.0	298	1.5	177.3	[145]
GO/PEI-hydrogels	Methylene blue	10	–	298	4	334	[105]
Polyquinone/graphene	Alizarin red C	100	6.0	298	2	3,290	[215]
RGO/rare-earth-metal-oxide	Rhodamine B	100	6,0	–	24	243.4	[216]
Aminated guar gum/GO	Rhodamine B	10-50	3.0–11.0	298	2	50.1	[217]
RGO/$CoFe_2O_4$	Rhodamine B	0.3	7.0	298	–	122	[218]
Graphene-tannic acid	Rhodamine B	8.0–512	11.0	298		201	[219]
Polyamine-modified magnetic-GO	Methyl violet	25–250	7.0	298	2	243	[220]
Polyamine-modified magnetic-GO	AR88	50–200	4.0	298	2	303	[220]
3D graphene nanosheets	Methyl orange	50–300	2.0	300	1	27.93	[221]
Chitosan/gelatin/graphene	Orange II	10–50	3.0	298	3	72.20	[222]
GO	Cationic blue	50–350	–	333	3	3933.91	[223]
GO/1-OA	Eriochrome blue	50–150	2.0–10.0	298	48	1189.10	[224]
GO/1-OA	Malachite green	50–150	2.0–10.0	298	48	2687.56	[224]
Magnetic/chitosan/GO	Disperse blue 367	60	2.0	363	2	298.27	[225]
Graphene-chitosan	Eosin Y	0–80	7.0	294	36	326	[226]
GO-activated carbon	Crystal violet	10–60	9.0	333	1.5	70	[213]
Graphene-Fe_3O_4	Crystal violet	10–40	2.0–10.0	298	0–300	460	[227]
Graphene-SO_3H/Fe_3O_4	Neutral red	20–250	6.0	298	–	216.8	[228]
Magnetic GO/hydrogel	Congo red	20–200	5.0–8.0	293	24	101.74	[143]
Nano-hydroxyapatite@GO	Congo red	–	3.0–12.0	298	1	48.5	[229]

67 (ZIF-67) polyhedrons were embedded on 3D RGO *via* self-assembly and produced a high-capability and broad-spectrum 3D RGO/ZIF-67 aerogels for the removal of CV and MO from aqueous solution [210]. The maximum adsorption capacity was recorded as 1714.2 mg/g and 426.3 mg/g for CV and MO, respectively. High removal of cationic CV dyes was mainly attributed to π-π interactions and electrostatic interactions between aerogel and dye molecules, and the synergistic effects at the interface of 3D RGO and ZIF-67 polyhedrons.

In another work, a pH-responsive magnetic GO/poly(*N*-vinylimidazole-*co*-acrylic acid) hydrogels (MGO/PNA) was fabricated by Yao *et al.* [211], and manifested very high adsorption capability of 609.8, 625.0, 613.5 and 609.8 mg/g for MV, MB, tartrazine (TZ), and amaranth (AR), respectively. Removal rate of cationic dyes (MB, MV) and anionic dyes (TZ, AR) were peaked at pH 12.0 and pH 2.0, respectively, due to electrostatic interactions between chromogenic groups of dyes and carboxyl groups of hydrogels. More recent studies in the adsorption of dyes onto graphene adsorbents are presented in Table 3 [105,143,145,212–229].

3.2.2. Adsorption of polycyclic aromatic hydrocarbons (PAHs)

Polycyclic aromatic hydrocarbons (PAHs) are organic pollutants composed of two or more combined benzene rings, having comparatively high desorption activation energy [230]. Due to very stable chemical structure and less bioavailable fraction, PAHs are not easily degraded by natural processes and remain unchanged in the environment for a long period of time [231]. Graphene adsorbents can efficiently remove PAHs compound from aqueous solution through numerous adsorption mechanisms, *i.e.*, π-π interactions, hydrophobic interactions, electrostatic interactions, H-bonding, Lewis acid-base, van der Waals interactions, surface attractions, *etc.* [13,232]. Out of these, π-π interactions and hydrophobic interactions are predominate in the most of PAHs adsorption [233,234].

Generally, the removal performance of PAHs varies significantly according to several physiochemical properties of both graphene and PAHs, such as chemical structure, hydrophobicity, surface functional groups, *etc.* [13]. Adsorption of PAHs onto graphene adsorbents increases with a decrease in their solubility and/or an increase in their hydrophobicity in solution [235]. The abundant oxygen-containing functional groups on GO surface decrease its hydrophobicity and increase the dispersion rate in aqueous solution. These functional groups are somewhat responsible for lessening adsorption sites for PAHs by bonding with water clusters. Consequently, pristine graphene and RGO have a tendency to show high removal capacity for PAHs than GO [193,236]. For instance, Sun *et al.* [237] compared the adsorption capacity of GO and RGO at neutral pH by naphthalene (NAP), anthracene (ANT) and pyrene (PYR). The results revealed that 95% and 60% of NAP were adsorbed on RGO and GO, respectively. Due to less oxygen-containing functional groups, the adsorption of PAHs on RGO was independent; whereas it was pH dependent in the case of GO.

Because of having more active sites, wrinkles and holes, graphene surface show high adsorption affinities for PAHs by sieving effect of the groove regions. However, the size of molecules significantly affects the adsorption of PAHs on graphene [132]. Generally, the adsorption affinities of smaller molecules onto graphene are relatively higher than large molecules, which claim that most adsorption sites on the groove regions are accessible for smaller molecules. Hence, it is advisable to consider the sieving effect due to the accessibility of molecules with dissimilar sizes [232].

In addition, the aromaticity (the number and spatial arrangement of aromatic rings) has crucial effects on the adsorptive interaction between PAHs and graphene, where the π-π dispersion is dominant mechanism [193,238]. Adsorption affinity of PAHs towards graphene has proven to be increased with the increasing number of aromatic rings in the structure. For example, phenanthrene (three benzene rings) exhibited greater sorption affinity to graphene than that of biphenyl (two benzene rings) *via* strong π-π interactions because of enhanced number of aromatic rings [193]. In the same way, Wang *et al.* [39] reported that the adsorption rate of 1-naphthol (two benzene rings) is faster than 2–4 dichlorophenol (single benzene ring) onto graphene, which was attributed to the higher π-π interaction between 1-naphthol and the graphene surface.

The adsorption performances of graphene toward PAHs are also affected by the solution pH. Graphene exhibits low sorption capacity for PAHs at low pH [239]. The properties of graphene in solution is governed by its point of zero charge (pH_{pzc}) measured by zeta potential analysis. Owing to deprotonation of hydroxyl and carboxyl groups, the net charge on graphene surfaces become negative at pH above pH_{pzc}, which facilitates the electrostatic interactions with positively charged PAHs molecules. On the contrary, at pH value under the pH_{pzc}, the net charge on graphene surfaces become positive, resulting high electrostatic repulsion with positively charged PAHs [239].

Graphene composites exhibit improved chemical and physical properties for removing PAHs from aqueous solutions [43]. Three magnetic graphene composites, such as magnetic graphene oxide (MGO), magnetic chemically-reduced graphene (MCRG) and magnetic annealing-reduced graphene (MARG) were synthesized and compared their adsorption capacities for phenanthrene [29]. The maximum adsorption capacities of three developed composites as follows: MCRG (43.00 mg/g) > MGO (28.17 mg/g) > MARG (23.29 mg/g). The highest adsorption capacity of MCRG for phenanthrene was mainly attributed to the larger surface area, pore volume, and numerous wrinkles of MCRG. Surface adsorption and pore-filling were the dominant mechanisms for the adsorption of phenanthrene onto MARG, whereas π-π interactions for MGO and MCRG.

In another study, Zheng *et al.* [240] designed β-cyclodextrin decorated GO (β-CD-GO) nanocomposites by *in situ* aggregation and employed to remove 1-naphthol from solution. The maximum adsorption capacity of β-CD-GO composites was recorded as 207.66 mg/g at 293 K. Surface complexation, π-π interaction, H-bonding were reported as the dominant mechanisms for the adsorption of 1-naphthol using hydroxyl and carboxyl functional groups on the surface of the β-CD-GO. Zhao *et al.* [241] also reported high removal rate (6.4 mmol/g) of 1-naphthol by sulfonated graphene nanosheets at 303 K. Bayazit *et al.* [242] prepared graphene nanoplatelet supported MIL-101 composites (GNP/MIL-101), and stated a rapid and high removal efficiency (93%) for naphthalene at 298 K. The π-π interaction was reported to be the principal mechanisms for adsorption. Table S2 (Supporting information) listed more studies that have been conducted to eliminate PAHs by different graphene adsorbents.

3.2.3. Adsorption of antibiotics

Antibiotics are introducing to the environment mainly through hospital wastes, pharmaceutical industries and veterinary drugs [243]. Because of large-scale consumption, they are gradually discharged into municipal wastewater or directly deposited in landfills, eventually, enter into the freshwater system, and exert detrimental impacts on living beings [244,245]. Apart from several conventional adsorbents, graphene and their nanocomposites achieved huge attention as emerging and high effective agents for eliminating antibiotics owing to their outstanding adsorption performances [246]. Peng *et al.* [247] acknowledged that the removal efficiency of antibiotics by graphene adsorbents is relatively higher than other conventional adsorbents. Table S3 (Supporting information) listed recent studies of graphene adsorbents on antibiotics.

Like other organic pollutants, antibiotic removal capability of graphene varies significantly depending on the structure and surface functional group presents on both graphene and antibiotic surface [244]. Moreover, parameters such as temperature, pH, contact time, initial concentration, and ionic strength could affect the adsorption behavior of antibiotic to different extents [248]. Rostamian *et al.* [249] reported that the adsorption rate of tetracycline (TC), doxycycline (DC) and ciprofloxacin (CP) onto GO nanosheets varied significantly because of dissimilarities in structure and functional group of antibiotics. The maximum removal capacity was recorded to be in the following order: CP (173.40 mg/g) > DC (116.50 mg/g) > TC (96.97 mg/g). CP displayed faster and highest adsorption rate compared to DC and TC due to its planer configuration, which exposed more active sites for π-π staking between GO and CP. In another work, Chen *et al.* [250] evaluated the adsorption rate of sulfamethoxazole (SMX) onto graphene and was found to be affected by the degree of functionalization, pH and ionic strength. The authors reported variations in the adsorption rate of sulfamethoxazole (SMX) with different functional materials in the following order: Pristine graphene (239.0 mg/g) > graphene-NH_2 (40.6 mg/g) > graphene−COOH (20.5 mg/g) > graphene−OH (11.5 mg/g).

Magnetic-graphene composites are well-known for their effective adsorption and desorption capacity to antibiotic molecules in aqueous solution. Miao *et al.* [251] prepared magnetic graphene oxide (MGO) and reported high adsorption capacity for chlortetracycline (CTC), oxytetracycline (OTC) and tetracycline hydrochloride (TC) as 303.95 mg/g, 289.85 mg/g, and 141.44 mg/g, respectively. Ionic forms of OTC and TC were found to be changed at low pH that reduces their uptake as a result of electrostatic repulsion by MGO. Nitrilotriacetic acid functionalized MGO (NDMGO) revealed enhanced sorption capacity to TC (212 mg/g), which was two times higher than pristine GO (109 mg/g) and three times higher than pure MGO (72 mg/g), respectively. This high removal rate might be ascribed to abundant amino and carboxyl functional groups generated on NDMGO surface [252].

Zhou *et al.* [253] synthesized biochar (citrus peel-derived) based magnetic GO (MGOCP) composites by a facile one-pot hydrothermal method and applied for efficient removal of ciprofloxacin CIP and sparfloxacin (SPA). The MGOCP achieved outstanding adsorption capacity for CIP (283.44 mg/g) and SPA (502.37 mg/g), respectively, which was almost 2 times higher than pure MCP. Liu *et al.* [245] fabricated genipin-crosslinked chitosan/magnetic GO-SO_3H (GC/MGO-SO_3H) composites. The maximum adsorption capacity for ibuprofen and tetracycline was reported to be increased from 113.27 mg/g to 138.16 mg/g and 473.25 mg/g to 556.28 mg/g with the increase in temperature from 298 K to 313 K, respectively.

3D derivatives of graphene, such as sponges, aerogels, hydrogels, *etc*. have gained huge interest in antibiotic elimination compared to other graphene composites, and a lot of works were conducted throughout the last couple of years [59,244]. Graphene hydrogel (GH) synthesized by one-step hydrothermal reduction displayed higher adsorption capacity (294.30 mg/g) for CP, which was higher than its precursor GO, reported by Sun *et al.* [254]. Since most of the oxygenated functional groups were removed by chemical reduction during synthesis process, H-bonding, hydrophobic interactions and π-π EDA interactions were identified as principal adsorption mechanisms.

Yu *et al.* [255] prepared magnetic graphene oxide sponge (MGOS) and used for adsorptive removal of TC in aqueous solution. The maximum removal rate of TC was achieved as 473 mg/g, which was 12 times higher than GO-magnetic composites developed by Lin *et al.* [256]. Enhanced removal of antibiotics was reported by introducing MOF onto graphene aerogel structure due to its huge surface area and high porosity [257]. The authors presented an easy preparation route for the *in situ* growth of ZIF-67 crystals on alginate-graphene (AG) substrate and designed AG-ZIF aerogels. The developed aerogels revealed outstanding adsorption capacities for TC (456.62 mg/g), which was much higher than pure alginate/graphene hydrogel (290.70 mg/g) reported by Zhuang *et al.* [258].

3.2.4. Adsorption of phenols

Phenols are a class of organic pollutants with one or more hydroxyl groups bonded to benzene ring [259]. Phenols can be entered into the environment through wastewater from several industries, *i.e*., paint, fertilizers, coal conversion, plastics, rubbers, pharmaceuticals, surfactants, and antioxidants [260]. Like other organic impurities, phenols also tend to persist in the environment for long period of time, thus, exert harmful impacts to human and animal [261].

Adsorptive removal of phenolic compounds is a bit difficult because of their low solubility and co-occurrence in multiple figures that increase competitive or co-operative effects in solution [262]. Compared to other conventional adsorbents, graphene displays selective adsorption ability to phenolic compounds with benzene rings through strong π-π interaction, because of having delocalized π-electron system [263]. For example, Gaber *et al.* [264] compared the phenol adsorption capacity of graphene with three different commercial activated carbon (AC), such as W-35, RB_2H_2, and nuchar granular AC. Graphene showed higher removal efficiency (72%) than W-35 AC (65%) at low temperature because of strong π-π interactions. The maximum Langmuir adsorption capacity was reported to be following order: Graphene (233 mg/g) > W-35 (200 mg/g) > nuchar granular (167 mg/g) > RB_2H_2 (91 mg/g).

Xu *et al.* [265] separated bisphenol A (BPA) from solution by graphene nanosheet with Langmuir adsorption capacity of 182 mg/g at 302.15 K, which was much higher than shown by other conventional adsorbents like CNTs (46.18 mg/g) [266], AC (9.1324 mg/g) [267], magnetic carbon nano-ions (65.77 mg/g) [268]. The high sorption capacity was attributed to π-π interaction and H-bonding caused by single-layer graphene planes with aromatic rings and the residual oxygenated functional groups.

Several studies revealed that graphene and RGO display enhanced removal performances to phenolic compounds than GO. Bele *et al.* [269] conducted a comparative study on graphene, GO and RGO for adsorptive removal of BPA in aqueous solution. The BPA removal rate was reported to be increased with increasing the reduction degree of GO with the following order: GO (17.27 mg/g) < RGO (80.81 mg/g) < graphene (94.06 mg/g). Wang *et al.* [39] also confirmed that adsorption capacity of RGO for different phenolic compounds increased with the degree of reduction. This is due to less oxygen-containing functional groups, which negatively affect the adsorption process. With decreasing the amount of functional groups, π-π interaction between graphene and phenols become stronger, resulting very high sorption efficiency. Wang *et al.* [270] further proved that RGO (197.7 mg/g) own higher adsorption capacity than GO (8.48 mg/g) in removing BPA from solution.

Apart from pure GO, 3D foam-like GO provides better performances to phenols due to its intrinsic corrugations, topological defects, vacancies, edges/cracks and adsorbed impurities, which facilitate mass transfer a lot [271]. Wang *et al.* [272] synthesized a nanoporous 3D GO using a simple sugar-blowing and post oxidation modification route, and manifested very high removal capacity to a variety of phenolic compounds, such as phenol (135.6 mg/g), 2-chlorophenol (2-CP) (191.3 mg/g), 4-chlorophenol (4-CP) (237.7 mg/g), 2,4 dichlorophenol (DCP) (398.6 mg/g), BPA (420.9 mg/g) and 2,4,6-trichlorophenol (TCP) (585.8 mg/g) at 25 °C.

Moreover, lots of paper reported improved sorption capacity of GO, when functionalized with nanoparticles, or polymers

[273,274]. Zhou *et al.* [262] designed PVAm-functionalized magnetic GO-(o-MWCNTs)-Fe_3O_4 nanocomposites and reported very high sorption capacity for phenol (224.21 mg/g), which was far greater than pristine GO (10.23 mg/g) reported by Mukherjee *et al.* [275]. Zhang *et al.* [276] demonstrated high elimination rate of phenolic compounds by GO/manganese oxide composites, synthesized *via in situ* (GO/MnO_X) and *ex situ* (GO/MnO_2) methods. GO/MnO_X exhibited higher adsorption capacities for *p*-cresol (*p*-CR) (107.68 mg/g) and *p*-*tert*-butylphenol (*p*-TBP) (135.41 mg/g) than GO/MnO_2 composites (98.64 mg/g for *p*-CR and 121.86 mg/g for *p*-TBP). This is due to the weak bonds between GO and MnO_2 which were not sufficient to promote interactions with pollutants and achieve required synergistic effect between adsorption and oxidation. Table S4 (Supporting information) presented other studies conducted on adsorptive removal of phenols by graphene adsorbents.

4. Desorption and regeneration of graphene adsorbents

An ideal adsorbent should have not only the high adsorption capacity for pollutants but also the high desorption and regeneration ability to reduce the cost of treatment. Reusability is therefore an important economic factor. Desorption and regeneration of graphene adsorbents vary widely along with the type of pollutant adsorb. However, for efficient desorption, selection of an appropriate eluent is crucial, which generally depends on the adsorption mechanism as well as the nature of both adsorbates and adsorbents [277].

Generally, alkaline and/or acid solution are commonly used to separate metal ions from the spent graphene, where pH of the solution plays major role in the mechanism [44]. The presence of oxygen-containing functional group on GO and RGO exhibits different protonation's at different pH. Moreover, ionization of pollutants can be easily controlled by changing of pH in solution. Hence, by regulating pH through addition of alkaline or acid solution, metal ions could be easily separated from spent adsorbents. For instance, Xu *et al.* [278] reported high desorption ability of GO cross-linked high-gluten flour (HGF) composites from Nd(III) using 0.1 mol/L HNO_3 solution as desorption agent. The adsorption efficiency was remained constant of 100%, even after five cycles. Zhang *et al.* [279] used 0.1 mol/L HCl solution for the separation of Cr(VI) from spent RGO/NiO, and reported the adsorption efficiency of 83% after five consecutive desorption cycles, which specified that HCl has excellent elution ability. In another study, Yi *et al.* [280] desorbed Cu(II) by 0.3 mol/L HCl and UO(II) by 0.3 mol/L HNO_3 from GO encapsulated polyvinyl alcohol/sodium alginate (SPG) hydrogel, and tested the reusability performance of the SPG with five cycles experiments. The removal efficiency for Cu(II) and UO(II) was decreased after the first adsorption-desorption cycle and then surprisingly remain constant without significant variation until the fifth cycle.

For the separation of organic molecules, hydrophobic solution could be effective eluent. Due to hydrophobicity, these eluents can be highly dissolved with organic pollutants rather than water, and eventually, separated with targeted pollutant from spent adsorbent. Soleimani *et al.* [281] isolated MB and RhB from GO-cellulose nanowhiskers (GO-CNW) using ethanol as eluent. After 3 adsorption-desorption recycling, the removal efficiency decreased little from the initial value of 100% to 95% for MB and 95% to 85% for RhB. Desorption of 3D GO-NiFe layered double hydroxide (GO-NiFe LDH) composites from MO was studied by Zheng *et al.* [282]. To regenerate GO-NiFe LDH, the adsorbent was eluted by methanol solution and the removal efficiency for MO was recorded to decrease from 97% to 81.3% after four consecutive cycles. Tian *et al.* [35] regenerated amino-functionalized polypropylene nonwoven/GO (PP-g-DMAEMA/GO) hybrid using ethanol as desorption agent. After five consecutive adsorption-regeneration cycles, the removal rate of BPA was recorded as 80.42%.

Another antique strategy for the separation of organic pollutants from spent adsorbent is burning the pollutant directly. Thermal conductivity of graphene materials is very high, and they can be stable at high temperature. On the other hand, organic pollutants would burn or evaporate at high temperature. Therefore, graphene adsorbents can be easily separated from organic pollutant by burning the composites on fire [283,284]. Bi *et al.* [285] recovered RGO after the adsorption of toluene and dodecane by burning the adsorbent on fire. Adsorption capacity of recovered RGO sponge remains over 99% even after the 10 times burning on fire. Similarly, Wu *et al.* [286] separated RGO from acrylonitrile, *p*-toluenesulfonic acid, 1-naphthalenesulfonic acid, and MB by heating the adsorbent at 450 °C for 100 min. After five cycles, the adsorption capacity of RGO for MB was remain constant.

Recently, magnetic separation has attracted considerable research interest because of easy and fast desorption and regeneration capacity [287]. In this technique, spent adsorbents are separated by applying an external magnetic field, and the supernatant is discarded [288]. For example, Liu *et al.* [289] retrieved xanthated Fe_3O_4-CS-GO from Cu(II) using aqueous Na_2EDTA and with the aid of an external magnet. The kinetic data revealed that the maximum desorption was approached in less than 50 min, and the adsorption capacity of regenerated composites was slightly reduced after five cycles. Fe_3O_4@GO hybrid was separated efficiently from MB and RhB using ethanol and external magnet field [290]. First, the dye-adsorbed Fe_3O_4@GO hybrid was separated from the aqueous solution using a magnet and then washed with ethanol solution several times. After the fifth cycle, the percent dye removal rates for RhB was recorded above 95% and was above 85% even after the eighth cycle. For MB, it was nearly 100% after second cycle and was above 65% even after the fifth cycle.

5. Conclusion and future research outlook

After carefully reviewing the whole paper, it is clearly observed that the graphene and their derivatives have been come out as promising adsorbents for wastewater decontamination. In the same way, graphene composite materials have drawn further attention than pristine graphene, GO and RGO owing to their enhanced adsorption and desorption capacities. Despite a large number of research work have been done on the adsorption technology with graphene materials, still the large-scale production of graphene adsorbents with low-cost is being viewed as a daunting challenge to the researchers. Likewise, in most of literatures, graphene adsorbents have been tested for merely one or two pollutants, where competitive adsorption capacity and selectivity of developed adsorbents were not comprehensively examined. As the industrial effluent contains multiple pollutants, it is crucial to investigate the simultaneous removal of many co-existing pollutants from multicomponent solution. Besides, through the recent years, more than hundreds of graphene composites have been synthesized and tested for a wide range of toxic pollutants, which does not allow the finding of best material. Hence, the laboratory techniques should be standardized in order to compare and identify the best material among many.

Most applications of graphene adsorbents are limited to only batch adsorption studies in laboratory stages rather than industrial-scales due to cost-effectiveness and technological challenges (*e.g.*, large-scale production, initial system set-up). Therefore, future research work should be carried out focusing on the development of low-cost and highly potential graphene adsorbent as well as verifying the performances at the pilot-scales to ascertain their commercial application. In order for these

to be achieved, we would like to highlight some recommendations to take into account while designing graphene adsorbents that might help in future research work.

(1) Design of 3D graphene is a new research trend in which graphene sheets are rearranged to obtain a 3D configuration. This type of structural arrangement helps to prevent agglomeration and ameliorate adsorption by providing a huge surface area and more porous network.
(2) Dispersion rate of adsorbent in the solution is crucial for adsorption. Homogenously-dispersed graphene adsorbent shows faster sorption kinetics; but, it suffers from the complicated separation from treated water. In that case, magnetic separation through an external magnetic field could be an effective solution through the development of magnetic-graphene composites. Magnetic separation also overcomes the hassles associated with the centrifugation, filtration, or gravitational separation.
(3) Wastewater contains not only organic and inorganic pollutants but also a variety of harmful microorganisms. Most of the graphene adsorbents reviewed in the literature, merely tested for eliminating organic and inorganic pollutants except few, which ultimately hindered their commercial application considering the economic aspects. In order to make the treatment process cost-effective, it is highly recommended to develop multifunctional graphene adsorbents for the joint removal of pollutants and microorganisms present in wastewater.
(4) The physicochemical properties of pollutants have significant influences on the performance of adsorbents under different experimental conditions. Hence, the chemical structure, bonding mechanism, solubility, volatility, sorption potential of different pollutants should be thoroughly investigated prior to develop the graphene adsorbents in order to boost their adsorption efficiency.
(5) The preparation methods for graphene adsorbents should be more simple, robust, and efficient. Besides, low production costs along with high removal efficiency of graphene adsorbents are always preferred to make the treatment process fully economic. Concurrently, several parameters of the adsorption experiment should be carefully optimized.
(6) Last but not least concern is the bio-safety and biocompatibility of graphene adsorbents. There is high possibility of releasing graphene to the environment during the production, use, and recycling. Therefore, the toxicity of graphene adsorbents must be comprehensively explored for human, animals and environment. Precautionary measures should be taken while designing the formula of adsorbents in order to alleviate their environmental toxicity.

Finally, despite the limitations, graphene adsorbents have boundless prospects in wastewater purification. Proper extensive research will make graphene adsorbent a "rising star" in the field of wastewater purification in near future.

Declaration of competing interest

The authors declare that they have no known competing financial interests or personal relationships that could have appeared to influence the work reported in this paper.

Acknowledgments

The authors would like to express their sincere gratitude to the National Natural Science Foundation of China (No. 51778230), National Key Research and Development Program (No. 2017YFB06026), Shanghai Rising-Star Program (No. 17QA1401000), and the Fundamental Research Funds for the Central Universities for their financial support (No. 222201718003).

Appendix A. Supplementary data

Supplementary data associated with this article can be found, in the online version, at https://doi.org/10.1016/j.cclet.2020.05.011.

References

[1] A.M. Awad, R. Jalab, A. Benamor, et al., J. Mol. Liq. 301 (2020) 112335.
[2] X. Yi, N.H. Tran, T. Yin, et al., Water Res. 121 (2017) 46–60.
[3] M. Huber, A. Welker, B. Helmreich, Sci. Total Environ. 541 (2016) 895–919.
[4] Y. Zhou, Q. Liu, J. Lu, et al., J. Hazard. Mater. 393 (2020) 122414.
[5] C.Y. Tang, P. Yu, L.S. Tang, et al., Ecotoxicol. Environ. Saf. 165 (2018) 299–306.
[6] Y. Zhou, J. He, J. Lu, et al., Chin. Chem. Lett. (2020), doi:http://dx.doi.org/10.1016/j.cclet.2020.02.008.
[7] Z.N. Garba, I. Lawan, W. Zhou, et al., Sci. Total Environ. 717 (2019) 135070.
[8] J. Lu, Y. Zhou, J. Lei, et al., Chemosphere 251 (2020) 126402.
[9] Y. Zhou, J. Lu, Q. Liu, et al., J. Hazard. Mater. 384 (2020) 121267.
[10] Y. Zhou, X. Gu, R. Zhang, J. Lu, Ind. Eng. Chem. Res. 53 (2014) 887–894.
[11] Y. Zhou, Y. Hu, W. Huang, et al., Chem. Eng. J. 341 (2018) 47–57.
[12] Q. Yang, B. Wang, Y. Chen, et al., Chin. Chem. Lett. 30 (2019) 234–238.
[13] G. Ersan, O.G. Apul, F. Perreault, T. Karanfil, Water Res. 126 (2017) 385–398.
[14] C. Santhosh, V. Velmurugan, G. Jacob, et al., Chem. Eng. J. 306 (2016) 1116–1137.
[15] Z. Li, L. Sellaoui, D. Franco, et al., Chem. Eng. J. 389 (2020) 124467.
[16] A. Yazidi, M. Atrous, F.E. Soetaredjo, et al., Chem. Eng. J. 379 (2020) 122320.
[17] M. Chauhan, V.K. Saini, S. Suthar, J. Clean. Prod. 258 (2020) 120686.
[18] Q. Huang, K. Chai, L. Zhou, H. Ji, Chem. Eng. J. 387 (2020) 124020.
[19] Q. Liu, Y. Li, H. Chen, et al., J. Hazard. Mater. 382 (2020) 121040.
[20] M. Hong, L. Yu, Y. Wang, et al., Chem. Eng. J. 359 (2019) 363–372.
[21] Y. Zhou, G. Cheng, K. Chen, et al., Ecotoxicol. Environ. Saf. 170 (2019) 278–285.
[22] G. Bottari, M.Á. Herranz, L. Wibmer, et al., Chem. Soc. Rev. 46 (2017) 4464–4500.
[23] R. Raccichini, A. Varzi, S. Passerini, B. Scrosati, Nat. Mater. 14 (2015) 271–279.
[24] M. Yusuf, M. Kumar, M.A. Khan, et al., Adv. Colloid Interface Sci. 273 (2019) 102036.
[25] K.S. Novoselov, A. Geim, Nat. Mater. 6 (2007) 183–191.
[26] A.K. Geim, Science 324 (2009) 1530–1534.
[27] K.S. Novoselov, V. Fal, L. Colombo, et al., Nature 490 (2012) 192–200.
[28] X. Lei, M. You, F. Pan, et al., Chin. Chem. Lett. 30 (2019) 2216–2220.
[29] D. Huang, B. Xu, J. Wu, et al., Chem. Eng. J. 368 (2019) 390–399.
[30] V. Kumar, K.H. Kim, J.W. Park, et al., Chem. Eng. J. 315 (2017) 210–232.
[31] S.M. Elgengehi, S. El-Taher, M.A. Ibrahim, et al., Appl. Surf. Sci. 507 (2020) 145038.
[32] H. Ahmad, Z. Huang, P. Kanagaraj, C. Liu, J. Hazard. Mater. 384 (2020) 121479.
[33] L. Zhao, J. Chen, N. Xiong, et al., Sci. Total Environ. 682 (2019) 591–600.
[34] L.C. Chen, S. Lei, M.Z. Wang, et al., Chin. Chem. Lett. 27 (2016) 511–517.
[35] J. Tian, J. Wei, H. Zhang, et al., Chem. Eng. J. 359 (2019) 852–862.
[36] Y. Li, J. Liu, L. Zhang, et al., Mater. Lett. 264 (2020) 127397.
[37] K. Thakur, B. Kandasubramanian, J. Chem. Eng. Data 64 (2019) 833–867.
[38] D. Chen, H. Feng, J. Li, Chem. Rev. 112 (2012) 6027–6053.
[39] X. Wang, S. Huang, L. Zhu, et al., Carbon 69 (2014) 101–112.
[40] S. Kim, C.M. Park, M. Jang, et al., Chemosphere 212 (2018) 1104–1124.
[41] S. Chowdhury, R. Balasubramanian, Adv. Colloid Interface Sci. 204 (2014) 35–56.
[42] F. Perreault, A.F. De Faria, M. Elimelech, Chem. Soc. Rev. 44 (2015) 5861–5896.
[43] J.-G. Yu, L.-Y. Yu, H. Yang, et al., Sci. Total Environ. 502 (2015) 70–79.
[44] X. Liu, R. Ma, X. Wang, et al., Environ. Pollut. 252 (2019) 62–73.
[45] M.M. Paixão, M.T.G. Vianna, M. Marques, Mater. Res. Express 5 (2018) 2053-1591.
[46] K.S. Novoselov, A.K. Geim, S.V. Morozov, et al., Science 306 (2004) 666–669.
[47] C.K. Chua, M. Pumera, Chem. Soc. Rev. 43 (2014) 291–312.
[48] R.S. Edwards, K.S. Coleman, Nanoscale 5 (2013) 38–51.
[49] Y. Sun, Q. Wu, G. Shi, Energy Environ. Sci. 4 (2011) 1113–1132.
[50] S. Haar, M. Bruna, J.X. Lian, et al., J. Phys. Chem. Lett. 7 (2016) 2714–2721.
[51] N. Behabtu, J.R. Lomeda, M.J. Green, et al., Nat. Nanotechnol. 5 (2010) 406–411.
[52] J.Y. Lim, N. Mubarak, E. Abdullah, et al., J. Ind. Eng. Chem. 66 (2018) 29–44.
[53] M.J. Allen, V.C. Tung, R.B. Kaner, Chem. Rev. 110 (2009) 132–145.
[54] X. Zhang, J. Ning, X. Li, et al., Nanoscale 5 (2013) 8363–8366.
[55] A. Ouerghi, M.G. Silly, M. Marangolo, et al., ACS Nano 6 (2012) 6075–6082.
[56] Y. Yang, R. Liu, J. Wu, et al., Sci. Rep. 5 (2015) 13480.
[57] V. Singh, D. Joung, L. Zhai, et al., Progr. Mater. Sci. 56 (2011) 1178–1271.
[58] X.J. Lee, B.Y.Z. Hiew, K.C. Lai, et al., J. Taiwan Inst. Chem. Eng. 98 (2019) 163–180.
[59] B.Y.Z. Hiew, L.Y. Lee, X.J. Lee, et al., Process Saf. Environ. Prot. 116 (2018) 262–286.
[60] T.B. Rouf, J.L. Kokini, J. Mater. Sci. 51 (2016) 9915–9945.

[61] W. Peng, H. Li, Y. Liu, S. Song, J. Mol. Liq. 230 (2017) 496–504.
[62] D.R. Dreyer, S. Park, C.W. Bielawski, R.S. Ruoff, Chem. Soc. Rev. 39 (2010) 228–240.
[63] W. Peng, H. Li, Y. Liu, S. Song, Appl. Surf. Sci. 364 (2016) 620–627.
[64] A. Reynosa-Martínez, G.N. Tovar, W. Gallegos, et al., J. Hazard. Mater. 384 (2020) 121440.
[65] B.C. Brodie, Philos. Trans. Roy. Soc. Lond. 149 (1859) 249–259.
[66] L. Staudenmaier, Ber. Deutsche. Chem. Ges. 31 (1898) 1481–1487.
[67] W.S. Hummers Jr, R.E. Offeman, J. Am. Chem. Soc. 80 (1958) 1339.
[68] D.C. Marcano, D.V. Kosynkin, J.M. Berlin, et al., ACS Nano 4 (2010) 4806–4814.
[69] R.K. Upadhyay, N. Soin, S.S. Roy, RSC Adv. 4 (2014) 3823–3851.
[70] N. Yadav, B. Lochab, FlatChem 13 (2019) 40–49.
[71] M. Sohail, M. Saleem, S. Ullah, et al., Mod. Electron. Mater. 3 (2017) 110–116.
[72] J. Chen, B. Yao, C. Li, G. Shi, Carbon 64 (2013) 225–229.
[73] H.J. Shin, K.K. Kim, A. Benayad, et al., Adv. Funct. Mater. 19 (2009) 1987–1992.
[74] S. Mao, H. Pu, J. Chen, RSC Adv. 2 (2012) 2643–2662.
[75] C. Li, Z. Zhuang, X. Jin, Z. Chen, Appl. Surf. Sci. 422 (2017) 469–474.
[76] R. Rajumon, J.C. Anand, A.M. Ealias, et al., J. Environ. Chem. Eng. 7 (2019) 103479.
[77] Z. Lin, X. Weng, L. Ma, et al., J. Colloid Interface Sci. 550 (2019) 1–9.
[78] Q. Wang, J. Li, Y. Song, X. Wang, Chem. Asian J. 8 (2013) 225–231.
[79] D. Krishnan, F. Kim, J. Luo, et al., Nano Today 7 (2012) 137–152.
[80] J.S. Cheng, J. Du, W. Zhu, Carbohydr. Polym. 88 (2012) 61–67.
[81] X. Huang, X. Qi, F. Boey, H. Zhang, Chem. Soc. Rev. 41 (2012) 666–686.
[82] Z.-F. Yang, L.-Y. Li, C.-T. Hsieh, et al., Mater. Chem. Phys. 219 (2018) 30–39.
[83] T. Esfandiyari, N. Nasirizadeh, M. Dehghani, M.H. Ehrampoosh, Chin. J. Chem. Eng. 25 (2017) 1170–1175.
[84] X. Luo, C. Wang, L. Wang, et al., Chem. Eng J. 22 (2013) 98–106.
[85] T.A. Saleh, A. Sarı, M. Tuzen, Chem. Eng J. 307 (2017) 230–238.
[86] X. Luo, C. Wang, S. Luo, et al., Chem. Eng J. 187 (2012) 45–52.
[87] W. Xu, Y. Chen, W. Zhang, B. Li, Adv. Powder Technol. 30 (2019) 493–501.
[88] M. Sun, J. Ma, M. Zhang, et al., Mater. Chem. Phys. 241 (2020) 122450.
[89] N.H. Othman, N.H. Alias, M.Z. Shahruddin, et al., J. Environ. Chem. Eng. 6 (2018) 2803–2811.
[90] A. Azizi, E. Moniri, A. Hassani, et al., Microchem. J. 145 (2019) 559–565.
[91] K. He, G. Zeng, A. Chen, et al., Compos. Part B-Eng. 161 (2019) 141–149.
[92] S. Chang, Q. Zhang, Y. Lu, et al., Sep. Purif. Technol. 238 (2019) 116400.
[93] C. Puri, G. Sumana, Appl. Clay Sci. 166 (2018) 102–112.
[94] P. Hou, G. Xing, L. Tian, et al., Sep. Purif. Technol. 213 (2019) 524–532.
[95] L. Ai, J. Jiang, Chem. Eng. J. 192 (2012) 156–163.
[96] X. Yang, J. Li, T. Wen, et al., Colloids Surf. A Physicochem. Eng. Asp. 422 (2013) 118–125.
[97] B. Szczęśniak, J. Choma, M. Jaroniec, Micropor. Mesopor. Mat. 279 (2019) 387–394.
[98] S. Zeng, N. Gan, R. Weideman-Mera, et al., Chem. Eng J. 218 (2013) 108–115.
[99] Z. Song, Y.-L. Ma, C.-E. Li, Sci. Total Environ. 651 (2019) 580–590.
[100] J. Phiri, P. Gane, T.C. Maloney, Mater. Sci. Eng. B 215 (2017) 9–28.
[101] T. Kuilla, S. Bhadra, D. Yao, et al., Prog. Polym. Sci. 35 (2010) 1350–1375.
[102] B.M. Itapu, A.H. Jayatissa, Chem. Sci. Int. J. 23 (2018) 1–16.
[103] D. Xue, T. Li, Y. Liu, et al., React. Funct. Polym. 136 (2019) 138–152.
[104] Y. Liu, Y. Huang, G. Chen, et al., Anal. Chim. Acta 1015 (2018) 20–26.
[105] H. Guo, T. Jiao, Q. Zhang, et al., Nanoscale Res. Lett. 10 (2015) 272.
[106] J. Liu, K. Zhu, T. Jiao, et al., Colloids Surf. A Physicochem. Eng. Asp. 529 (2017) 668–676.
[107] N. Gan, J. Zhang, S. Lin, et al., Materials 7 (2014) 6028–6044.
[108] Y.L.F. Musico, C.M. Santos, M.L.P. Dalida, D.F. Rodrigues, J. Mater. Chem. A 1 (2013) 3789–3796.
[109] P.T. Yin, S. Shah, M. Chhowalla, K.B. Lee, Chem. Rev. 115 (2015) 2483–2531.
[110] Y. Vicente-Martínez, M. Caravaca, A. Soto-Meca, et al., Sci. Total Environ. 709 (2020) 136111.
[111] A.A. Kotp, A.A. Farghali, R.M. Amin, et al., J. Environ. Chem. Eng. 7 (2019) 102977.
[112] L. Fang, L. Xu, J. Li, L.-Z. Huang, Sci. Total Environ 683 (2019) 275–283.
[113] H. Zhou, T. Huang, D. Chen, et al., Sens. Actuators B Chem. 249 (2017) 405–413.
[114] J. Guo, R. Wang, W.W. Tjiu, et al., J. Hazard. Mater. 225 (2012) 63–73.
[115] A. Baruah, S. Mondal, L. Sahoo, U.K. Gautam, J. Solid State Chem. 280 (2019) 120963.
[116] S.-M. Alatalo, E. Daneshvar, N. Kinnunen, et al., Chem. Eng. J. 373 (2019) 821–830.
[117] J. Jin, Z. Yang, W. Xiong, et al., Sci. Total Environ. 650 (2019) 408–418.
[118] S.H. Alwan, H.A.H. Alshamsi, L.S. Jasim, J. Mol. Struct. 1161 (2018) 356–365.
[119] M.R. Abukhadra, M.A. Sayed, A.M. Rabie, S.A. Ahmed, Colloids Surf. A Physicochem. Eng. Asp. 577 (2019) 583–593.
[120] A. Al-Nafiey, M.H. Al-Mamoori, S.M. Alshrefi, R.T. Ahmed, Mater. Today Proceed. 19 (2019) 94–101.
[121] S. Li, Z. Niu, X. Zhong, et al., J. Hazard. Mater. 229 (2012) 42–47.
[122] F. Sharif, E.P. Roberts, Chemosphere 241 (2020) 125020.
[123] M. Daraee, E. Ghasemy, J. Environ. Chem. Eng. 8 (2020) 103836.
[124] C. Du, Y. Song, S. Shi, et al., Sci. Total Environ. 711 (2020) 134662.
[125] L. Qi, R. Xu, J. Gong, Talanta 209 (2020) 120523.
[126] C. Santhosh, E. Daneshvar, P. Kollu, et al., Chem. Eng. J. 322 (2017) 472–487.
[127] W. Czepa, D. Pakulski, S. Witomska, et al., Carbon 158 (2020) 193–201.
[128] Y. Ren, N. Yan, Q. Wen, et al., Chem. Eng. J. 175 (2011) 1–7.
[129] J. Tolasz, M. Štastný, V. Štengl, Mater. Today Proceed. 3 (2016) 2795–2806.
[130] L. Zhang, Y. Li, H. Guo, et al., Environ. Pollut. 248 (2019) 332–338.
[131] K. Wu, C. Jing, J. Zhang, et al., Appl. Surf. Sci. 466 (2019) 746–756.
[132] N. Baig, M. Sajid, T.A. Saleh, J. Environ. Manage. 244 (2019) 370–382.
[133] I. Ali, X. Mbianda, A. Burakov, et al., Environ. Int. 127 (2019) 160–180.
[134] X. Li, T. Lu, Y. Wang, Y. Yang, Chin. Chem. Lett. 30 (2019) 2318–2322.
[135] W. Huang, Y. Hu, Y. Li, et al., J. Taiwan Inst. Chem. Eng. 82 (2018) 189–197.
[136] C. Ling, Y. Zhao, Z. Ren, et al., Chin. Chem. Lett. 30 (2019) 2196–2200.
[137] Y. Dai, L. Niu, J. Zou, et al., Chin. Chem. Lett. 29 (2018) 887–891.
[138] H. Chen, Y. Zhou, J. Wang, et al., J. Hazard. Mater. 389 (2020) 121897.
[139] J.Z. Pirhaji, F. Moeinpour, A.M. Dehabadi, S.A.Y. Ardakani, J. Mol. Liq. 300 (2020) 112345.
[140] C. Bai, L. Wang, Z. Zhu, Int. J. Biol. Macromol. 147 (2020) 898–910.
[141] Q. Fang, X. Zhou, W. Deng, Z. Liu, Chem. Eng. J. 308 (2017) 1001–1009.
[142] H. Ahmad, C. Cai, C. Liu, Microchem. J. 145 (2019) 833–842.
[143] R. Sahraei, Z.S. Pour, M. Ghaemy, J. Clean. Prod. 142 142 (2017) 2973–2984.
[144] X. Yu, Y. Wei, C. Liu, et al., Chemosphere 222 (2019) 258–266.
[145] P.T.L. Huong, N. Tu, H. Lan, et al., RSC Adv. 8 (2018) 12376–12389.
[146] T.T.P.N.X. Trinh, D.T. Quang, T.H. Tu, et al., Synth. Met. 247 (2019) 116–123.
[147] S. Liu, H. Wang, L. Chai, M. Li, J. Colloid Interface Sci. 478 (2016) 288–295.
[148] M. Neelaveni, P.S. Krishnan, R. Ramya, et al., Adv. Powder Technol. 30 (2019) 596–609.
[149] X. Wang, J. Lu, B. Cao, et al., Colloids Surf. A Physicochem. Eng. Asp. 560 (2019) 384–392.
[150] N. Khare, J. Bajpai, A. Bajpai, Environ. Nanotechnol. Monit. Manag. 10 (2018) 148–162.
[151] P. Qiu, S. Wang, C. Tian, Z. Lin, Environ. Pollut. 252 (2019) 1133–1141.
[152] L. Cui, X. Guo, Q. Wei, et al., J. Colloid Interface Sci. 439 (2015) 112–120.
[153] Y. Zhang, Y. Liu, X. Wang, et al., Carbohydr. Polym. 101 (2014) 392–400.
[154] L. Fan, C. Luo, M. Sun, et al., Colloids Surf. B. Biointerfaces 103 (2013) 523–529.
[155] T.Q. Dat, N.T. Ha, P. Van Thin, et al., IEEE Trans. Magn. 54 (2018) 1–6.
[156] H. Liu, S. Xie, J. Liao, et al., J. Radioanal. Nucl. Chem. 317 (2018) 1349–1360.
[157] L. Liu, C. Li, C. Bao, et al., Talanta 93 (2012) 350–357.
[158] Q. Liu, Y. Zhou, J. Lu, Y. Zhou, Chemosphere 241 (2019) 125043.
[159] X. Wang, B. Liu, Q. Lu, Q. Qu, J. Chromatogr. A 1362 (2014) 1–15.
[160] R. Sitko, E. Turek, B. Zawisza, et al., Dalton Trans. 42 (2013) 5682–5689.
[161] C.J. Madadrang, H.Y. Kim, G. Gao, et al., ACS Appl. Mater. Interfaces 4 (2012) 1186–1193.
[162] H. Wang, X. Yuan, Y. Wu, et al., Chem. Eng. J. 262 (2015) 597–606.
[163] M. Ahmaruzzaman, D. Sharma, J. Colloid Interface Sci. 287 (2005) 14–24.
[164] G. Zhao, X. Ren, X. Gao, et al., Dalton Trans. 40 (2011) 10945–10952.
[165] Z. Li, F. Chen, L. Yuan, et al., Chem. Eng. J. 210 (2012) 539–546.
[166] G. Zhao, T. Wen, X. Yang, et al., Dalton Trans. 41 (2012) 6182–6188.
[167] Q. Kong, S. Preis, L. Li, et al., Sep. Purif. Technol. 232 (2020) 115956.
[168] X. Zhu, Y. Shan, S. Xiong, et al., ACS Appl. Mater. Interfaces 8 (2016) 15848–15854.
[169] J. Ding, B. Li, Y. Liu, et al., J. Mater. Chem. a 3 (2015) 832–839.
[170] F. Yu, S. Sun, J. Ma, S. Han, Phys. Chem. Chem. Phys. 17 (2015) 4388–4397.
[171] M. Zhang, X. Ma, J. Li, et al., Chemosphere 234 (2019) 196–203.
[172] M.A. Malana, R.B. Qureshi, M.N. Ashiq, Chem. Eng. J. 172 (2011) 721–727.
[173] Y. Yoon, W.K. Park, T.M. Hwang, et al., J. Hazard. Mater. 304 (2016) 196–204.
[174] H. Su, Z. Ye, N. Hmidi, Colloids Surf. A Physicochem. Eng. Asp. 522 (2017) 161–172.
[175] B. Barik, A. Kumar, P.S. Nayak, et al., Mater. Chem. Phys. 239 (2020) 122028.
[176] K. Molaei, H. Bagheri, A.A. Asgharinezhad, et al., Talanta 167 (2017) 607–616.
[177] A. Sherlala, A. Raman, M. Bello, A. Asghar, Chemosphere 193 (2018) 1004–1017.
[178] C. Zhou, H. Zhu, Q. Wang, et al., RSC Adv. 7 (2017) 18466–18479.
[179] H.T. Xing, J.H. Chen, X. Sun, et al., Chem. Eng. J. 263 (2015) 280–289.
[180] N. Zhang, H. Qiu, Y. Si, et al., Carbon 49 (2011) 827–837.
[181] L. Zhang, H. Luo, P. Liu, et al., Int. J. Biol. Macromol. 87 (2016) 586–596.
[182] P. Sharma, A.K. Singh, V.K. Shahi, ACS Sustain. Chem. Eng. 7 (2018) 1427–1436.
[183] M.S. Samuel, J. Bhattacharya, S. Raj, et al., Int. J. Biol. Macromol. 121 (2019) 285–292.
[184] Y. Zhou, J. Lu, Y. Zhou, Y. Liu, Environ. Pollut. 252 (2019) 352–365.
[185] W. He, N. Li, X. Wang, et al., Chin. Chem. Lett. 29 (2018) 857–860.
[186] G.Z. Kyzas, E.A. Deliyanni, D.N. Bikiaris, A.C. Mitropoulos, Chem. Eng. Res. Des. 129 (2018) 75–88.
[187] W. Peng, H. Li, Y. Liu, S. Song, J. Mol. Liq. 221 (2016) 82–87.
[188] P. Bradder, S.K. Ling, S. Wang, S. Liu, J. Chem. Eng. Data 56 (2011) 138–141.
[189] S. Thangavel, G. Venugopal, Powder Technol. 257 (2014) 141–148.
[190] W. Konicki, M. Aleksandrzak, D. Moszyński, E. Mijowska, J. Colloid Interface Sci. 496 (2017) 188–200.
[191] G. Ramesha, A.V. Kumara, H. Muralidhara, S. Sampath, J. Colloid Interface Sci. 361 (2011) 270–277.
[192] C. Minitha, M. Lalitha, Y. Jeyachandran, et al., Mater. Chem. Phys. 194 (2017) 243–252.
[193] O.G. Apul, Q. Wang, Y. Zhou, T. Karanfil, Water Res. 47 (2013) 1648–1654.
[194] K. Gupta, O.P. Khatri, J. Colloid Interface Sci. 501 (2017) 11–21.
[195] N. Sykam, V. Madhavi, G.M. Rao, J. Environ. Chem. Eng. 6 (2018) 3223–3232.
[196] J. Xiao, W. Lv, Z. Xie, et al., J. Mater. Chem. a 4 (2016) 12126–12135.
[197] T.R. Das, P.K. Sharma, Mater. Sci. Semicond. Process. 105 (2020) 104721.
[198] M. Heidarizad, S.S. Şengör, J. Mol. Liq. 224 (2016) 607–617.
[199] P. Tan, Y. Hu, J. Mol. Liq. 242 (2017) 181–189.
[200] Y. Yang, W. Yu, S. He, et al., Appl. Clay Sci. 168 (2019) 304–311.
[201] S. Wang, X. Li, Y. Liu, et al., J. Hazard. Mater. 342 (2018) 177–191.
[202] B. Chen, Y. Liu, S. Chen, et al., J. Taiwan Inst. Chem. Eng. 67 (2016) 191–201.

[203] C. Li, H. Zhu, X. She, et al., RSC Adv. 6 (2016) 67242–67251.
[204] M.O. Ansari, R. Kumar, S.A. Ansari, et al., J. Colloid Interface Sci. 496 (2017) 407–415.
[205] S. Jayanthi, N.K. Eswar, S.A. Singh, et al., RSC Adv. 6 (2016) 1231–1242.
[206] R. Zambare, X. Song, S. Bhuvana, et al., ACS Sustain. Chem. Eng. 5 (2017) 6026–6035.
[207] J. Dai, T. Huang, S.-Q. Tian, et al., Mater. Des. 107 (2016) 187–197.
[208] Y.C. Shi, A.J. Wang, X.L. Wu, et al., J. Colloid Interface Sci. 484 (2016) 254–262.
[209] K.C. Lai, L.Y. Lee, B.Y.Z. Hiew, et al., J. Environ. Sci. 79 (2019) 174–199.
[210] Q. Yang, R. Lu, S. Ren, et al., Chem. Eng. J. 348 (2018) 202–211.
[211] G. Yao, W. Bi, H. Liu, Colloids Surf. A Physicochem. Eng. Asp. 588 (2020) 124393.
[212] S. Wang, H. Ning, N. Hu, et al., Compos. Part B-Eng. 163 (2019) 716–722.
[213] A. Abd-Elhamid, E.A. Kamoun, A.A. El-Shanshory, et al., J. Mol. Liq. 279 (2019) 530–539.
[214] A.Y. Sham, S.M. Notley, J. Environ. Chem. Eng. 6 (2018) 495–504.
[215] A. Burakov, E. Neskoromnaya, A. Babkin, Mater. Today Proceed. 11 (2019) 392–397.
[216] Y. Zhang, K. Li, J. Liao, Appl. Surf. Sci. 504 (2020) 144377.
[217] S. Gopi, A. Rajeswari, G. Sudharsan, A. Pius, J. Water Process. Eng. 31 (2019) 100850.
[218] W. Yin, S. Hao, H. Cao, RSC Adv. 7 (2017) 4062–4069.
[219] K. Liu, H. Li, Y. Wang, et al., Colloids Surf. A Physicochem. Eng. Asp. 477 (2015) 35–41.
[220] G. Abdi, A. Alizadeh, J. Amirian, et al., J. Mol. Liq. 289 (2019) 111118.
[221] L. Labiadh, A.R. Kamali, Appl. Surf. Sci. 490 (2019) 383–394.
[222] M. Wu, W. Chen, Q. Mao, et al., Chem. Eng. Res. Des. 144 (2019) 35–46.
[223] X. Jiao, L. Zhang, Y. Qiu, J. Guan, Colloids Surf. A Physicochem. Eng. Asp. 529 (2017) 292–301.
[224] M. Lv, L. Yan, C. Liu, et al., Chem. Eng. J. 349 (2018) 791–799.
[225] F. Taher, F. Kamal, N. Badawy, A. Shrshr, Mater. Res. Bull. 97 (2018) 361–368.
[226] Y. Chen, L. Chen, H. Bai, L. Li, J. Mater. Chem. A 1 (2013) 1992–2001.
[227] G. Bharath, E. Alhseinat, N. Ponpandian, et al., Sep. Purif. Technol. 188 (2017) 206–218.
[228] S. Wang, J. Wei, S. Lv, et al., CLEAN–Soil, Air, Water 41 (2013) 992–1001.
[229] S.M. Prabhu, A. Khan, M.H. Farzana, et al., J. Mol. Liq. 269 (2018) 746–754.
[230] S. Lamichhane, K.B. Krishna, R. Sarukkalige, Chemosphere 148 (2016) 336–353.
[231] K.-H. Shin, K.-W. Kim, Y. Ahn, J. Hazard. Mater. 137 (2006) 1831–1837.
[232] J. Wang, Z. Chen, B. Chen, Environ. Sci. Technol. 48 (2014) 4817–4825.
[233] G. Ersan, Y. Kaya, O.G. Apul, T. Karanfil, Sci. Total Environ. 565 (2016) 811–817.
[234] Y. Li, Q. Du, T. Liu, et al., Chem. Eng. Res. Des. 91 (2013) 361–368.
[235] X. Chen, B. Chen, Environ. Sci. Technol. 49 (2015) 6181–6189.
[236] B. Beless, H.S. Rifai, D.F. Rodrigues, Environ. Sci. Technol. 48 (2014) 10372–10379.
[237] Y. Sun, S. Yang, G. Zhao, et al., Chem. Asian J. 8 (2013) 2755–2761.
[238] Z. Pei, L. Li, L. Sun, et al., Carbon 51 (2013) 156–163.
[239] S. Wang, H. Sun, H.-M. Ang, M. Tadé, Chem. Eng. J. 226 (2013) 336–347.
[240] H. Zheng, Y. Gao, K. Zhu, et al., J. Colloid Interface Sci. 530 (2018) 154–162.
[241] G. Zhao, J. Li, X. Wang, Chem. Eng. J. 173 (2011) 185–190.
[242] Ş.S. Bayazit, M. Yildiz, Y.S. Aşçi, et al., J. Alloys Compd. 701 (2017) 740–749.
[243] S. Rodriguez-Mozaz, S. Chamorro, E. Marti, et al., Water Res. 69 (2015) 234–242.
[244] X. Wang, R. Yin, L. Zeng, M. Zhu, Environ. Pollut. 253 (2019) 100–110.
[245] Y. Liu, R. Liu, M. Li, et al., Carbohydr. Polym. 220 (2019) 141–148.
[246] A. Khan, J. Wang, J. Li, et al., Environ. Sci. Pollut. Res. 24 (2017) 7938–7958.
[247] B. Peng, L. Chen, C. Que, et al., Sci. Rep. 6 (2016) 31920.
[248] F. Yu, Y. Li, S. Han, J. Ma, Chemosphere 153 (2016) 365–385.
[249] R. Rostamian, H. Behnejad, Ecotoxicol. Environ. 147 (2018) 117–123.
[250] H. Chen, B. Gao, H. Li, J. Environ. Chem. Eng. 2 (2014) 310–315.
[251] J. Miao, F. Wang, Y. Chen, et al., Appl. Surf. Sci. 475 (2019) 549–558.
[252] M.F. Li, Y.-G. Liu, G.M. Zeng, et al., J. Colloid Interface Sci. 485 (2017) 269–279.
[253] Y. Zhou, S. Cao, C. Xi, et al., Bioresour. Technol. 292 (2019) 121951.
[254] Y. Sun, Y. Yang, M. Yang, et al., J. Mol. Liq. 284 (2019) 124–130.
[255] B. Yu, Y. Bai, Z. Ming, et al., Mater. Chem. Phys. 198 (2017) 283–290.
[256] Y. Lin, S. Xu, J. Li, Chem. Eng. J. 225 (2013) 679–685.
[257] Y. Kong, Y. Zhuang, K. Han, B. Shi, Colloids Surf. A: Physicochem. Eng. Asp. 588 (2020) 124360.
[258] Y. Zhuang, F. Yu, J. Ma, J. Chen, J. Colloid Interface Sci. 507 (2017) 250–259.
[259] X. Yang, R. Zou, F. Huo, et al., J. Hazard. Mater. 164 (2009) 367–373.
[260] W. Raza, J. Lee, N. Raza, et al., J. Ind. Eng. Chem. 71 (2019) 1–18.
[261] M. Al-Mamun, S. Kader, M. Islam, M. Khan, J. Environ. Chem. Eng. 7 (2019) 103248.
[262] K. Zhou, J. Zhang, Y. Xiao, et al., Chem. Eng. J. 389 (2020) 124223.
[263] A. Gulati, R. Kakkar, Chem. Eng. Res. Des. 153 (2020) 21–36.
[264] D. Gaber, M.A. Haija, A. Eskhan, F. Banat, Water Air Soil Pollut. 228 (2017) 320.
[265] J. Xu, L. Wang, Y. Zhu, Langmuir 28 (2012) 8418–8425.
[266] S. Li, Y. Gong, Y. Yang, et al., Chem. Eng. J. 260 (2015) 231–239.
[267] Q. Zhou, Y. Wang, J. Xiao, H. Fan, Synth. Met. 212 (2016) 113–122.
[268] M. Zhou, Q. Li, S. Zhong, et al., Mater. Chem. Phys. 198 (2017) 186–192.
[269] S. Bele, V. Samanidou, E. Deliyanni, Chem. Eng. Res. Des. 109 (2016) 573–585.
[270] P. Wang, D. Zhang, H. Tang, et al., J. Hazard. Mater. 371 (2019) 513–520.
[271] Y. Zhu, S. Murali, W. Ca, et al., Adv. Mater. 22 (2010) 3906–3924.
[272] W. Wang, Q. Gong, Z. Chen, et al., Chem. Eng. J. 378 (2019) 122085.
[273] S. Manna, S. Prakash, P. Das, Colloids Surf. A Physicochem. Eng. Asp. 581 (2019) 123818.
[274] P. Badhai, S. Kashyap, S.K. Behera, Environ. Nanotechnol. Monit. Manag. 13 (2020) 100282.
[275] M. Mukherjee, S. Goswami, P. Banerjee, et al., Environ. Technol. Innov. 13 (2019) 398–407.
[276] B. Zhang, R. Zhao, D. Sun, et al., J. Clean. Prod. 215 (2019) 165–174.
[277] G. Zhao, X. Huang, Z. Tang, et al., Polym. Chem. 9 (2018) 3562–3582.
[278] X. Xu, J. Zou, J. Teng, et al., Ecotoxicol. Environ. Saf. 166 (2018) 1–10.
[279] K. Zhang, H. Li, X. Xu, H. Yu, Microporous Mesoporous Mater. 255 (2018) 7–14.
[280] X. Yi, F. Sun, Z. Han, et al., Ecotoxicol. Environ. Saf. 158 (2018) 309–318.
[281] K. Soleimani, A.D. Tehrani, M. Adeli, Ecotoxicol. Environ. 147 (2018) 34–42.
[282] Y. Zheng, B. Cheng, W. You, et al., J. Hazard. Mater. 369 (2019) 214–225.
[283] J. Zhao, W. Ren, H.M. Cheng, J. Mater. Chem. 22 (2012) 20197–20202.
[284] Z. Geng, Y. Lin, X. Yu, et al., J. Mater. Chem. 22 (2012) 3527–3535.
[285] H. Bi, X. Xie, K. Yin, et al., Adv. Funct. Mater. 22 (2012) 4421–4425.
[286] T. Wu, X. Cai, S. Tan, et al., Chem. Eng. J. 173 (2011) 144–149.
[287] Y. Liu, H. Huang, D. Gan, et al., Ceram. Int. 44 (2018) 18571–18577.
[288] N. Li, H.L. Jiang, X. Wang, et al., Trac-Trend. Anal. Chem. 102 (2018) 60–74.
[289] J. Liu, W. Liu, Y. Wang, et al., Appl. Surf. Sci. 367 (2016) 327–334.
[290] V. Ganesan, C. Louis, S.P. Damodaran, J. Environ. Chem. Eng. 6 (2018) 2176–2190.